Impact of physical factors for attenuation correction in quantitative positron emission tomography images

Hye-Kyung Son

Department of Medical Science

The Graduate School, Yonsei University

Impact of physical factors for attenuation correction in quantitative positron emission tomography images

Directed by Professor Hee-Joung Kim

The Doctoral Dissertation submitted to the Department of Medical Science, the Graduate School of Yonsei University in partial fulfillment of the requirements for the degree of Doctor of Philosophy

Hye-Kyung Son

June 2005

This certifies that the Doctoral Dissertation of Hye-Kyung Son is approved.

Thesis Supervisor : Hee-Joung Kim

Thesis Committee : Nam Hyun Kim

Thesis Committee : Dong Goo Kim

Thesis Committee : Jong Doo Lee

Thesis Committee : Hyung Sik Yoo

The Graduate School

Yonsei University

June 2005

ACKNOWLEGDEMENTS

First of all, I thank the Lord. This dissertation and the effort of its pursuit are dedicated to Him.

I thank my dissertation advisor, Hee-Joung Kim for introducing me to medical physics and supporting me in my pursuit of this field. I learned much about physics in nuclear medicine under his considerate guidance. I specially thank Timothy G. Turkington for introducing me to this dissertation topic and providing me much advice and discussion. I thank my dissertation committees, Nam Hyun Kim, Dong Goo Kim, Jong Doo Lee, and Hyung Sik Yoo for providing me with the much needed advice. I thank our laboratory instructor, Haijo Jung for much advice. Thanks to all of nuclear medicine people for their help and advice. Thanks to all of our laboratory members for making my graduate school a great experience.

Finally, I would like to deeply thank my family for their endless love, support, and encouragement.

June 2005

Written by author

TABLE OF CONTENTS

LIST OF FIGURES

LIST OF TABLES

ABSTRACT

Impact of physical factors for attenuation correction in quantitative positron emission tomography images

Hye-Kyung Son

Department of Medical Science

The Graduate School, Yonsei University

(Directed by Professor Hee-Joung Kim)

Positron emission tomography is a unique and an analytical nuclear medicine imaging technology that uses positron-labeled compounds to visualize and measure many biological processes in living subjects. PET imaging provides a way of obtaining information non-invasively, while maintaining superior sensitivity in diagnosis, prognosis, and staging, as well as monitoring the effects of treatment. To improve the diagnostic accuracy of PET images, attenuation correction must be done by measuring attenuation factors. This is accomplished using a transmission source such as ^{68}Ge or ^{137}Cs, because the attenuation of photons is the most important factor in preventing the degradation of the PET image quality. Combined positron emission tomography/computerized tomography (PET/CT) scanners have been recently introduced, and it allows for both functional and anatomical images to be inherently co-registered. It is also possible to use the CT scan for attenuation

correction. Recent studies show that metallic materials and contrast agents can produce inappropriate FDG uptake in conventional and the CT-based attenuation correction, which can cause misinterpretation of PET images. The purpose of this dissertation was to study the impact of metallic materials and contrast agents in PET and PET/CT images. Simulation and experiments were done to study the severity of artifacts from aluminum and titanium when there is motion between emission and transmission scans. A variety of factors were evaluated, including size and density of the metallic materials, transmission and emission noise levels, image resolution, amount of shift, and transmission and emission processing. Simulation and experiments were done to study the effects of contrast agents. A variety of factors were estimated, including non-uniform enhancement of contrast agent, concentration and distribution size of contrast agent, noise level, image resolution, reconstruction algorithm, hypo-attenuation of contrast agent, and different time phases for contrast agent. The combination of motion between transmission and emission scans and small dense structures produced artifacts on attenuation-corrected PET images. The severity of the effects depends on a variety of factors, including the size and density of metallic materials, the transmission and emission noise levels, the amount of shift, and the transmission and emission processing. Contrast agents introduced artifacts and degraded image quality on the attenuation-corrected PET images. The severity of these effects depends on a variety of factors, including the concentration and distribution size of contrast agent, the noise levels, the image resolution, and the reconstruction algorithm. The non-

uniform enhancement of contrast agent in transmission map produced inappropriate hyper-uptake on the attenuation-corrected emission images. Hypo-attenuation of contrast agent in tumors can degrade the tumor intensity on the attenuation-corrected emission images and degradation of the tumor intensity is influenced by different time phases. Our simulation and experimental results indicated that the impact of metallic materials and contrast agents should be considered with a full understanding of their potential problems in clinical PET and PET/CT images.

Key Words: positron emission tomography, positron emission tomography/computed tomography, attenuation correction, artifacts, metallic materials, contrast agents

Impact of physical factors for attenuation correction in quantitative positron emission tomography images

Hye-Kyung Son

Department of Medical Science

The Graduate School, Yonsei University

(Directed by Professor Hee-Joung Kim)

I. INTRODUCTION

1. Positron emission tomography

Positron emission tomography (PET) is a unique and an analytical nuclear medicine imaging technology that uses positron-labeled compounds to visualize and measure many biological processes in living subjects[1-6].

Because proton-rich nucleus is unstable, they decay by electron capture and

positron (e^+) emission. The positron emission decays by emitting a positron which has the same mass as an electron but has a positive charge. For this decay mode, the minimum transition energy difference in total energy between parent and daughter states has to be at least 1.022 MeV. The equation for the positron emission can be represented as[1]:

$$ {}^{A}_{Z}X \rightarrow {}^{A}_{Z-1}X + e^{+} + \nu \qquad \text{Eq. 1-1} $$

where A is a mass number, Z is an atomic number, and ν is a neutrino.

After ejection from the nucleus, the positron loses its kinetic energy by scattering interactions with atomic electrons and comes to rest within a few millimeters from its origin. The positron then combines with an electron in an annihilation reaction, in which their mass converts into energy in the form of γ-rays. (Fig. 1.1). The energy released by the annihilation for each particle is 511 keV, which is emitted 180 degrees from each other. These two γ-rays are detected by two opposite detectors simultaneously within a coincidence timing window. By this coincident detection, it is possible to define the direction from which the γ-rays originate and thus it is called an electronic coincidence collimation. This is the basic principle of the PET imaging. Various positron emitting radioisotopes are shown in Table 1.1.

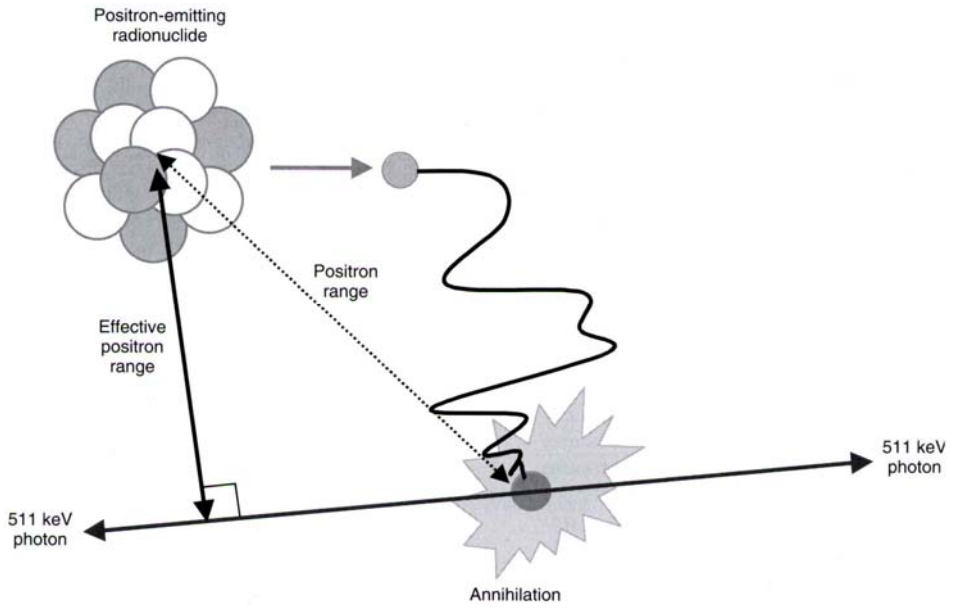

Figure 1.1. Schematic diagram of the annihilation reaction[2].

Table 1.1. Properties of commonly used positron emitting radioisotopes[2].

Isotope	Half-life	β^+ fraction	β^+ E_{max} (MeV)
^{18}F	1.83 h	0.97	0.64
^{11}C	20.4 min	0.99	0.96
^{13}N	9.96 min	1	1.19
$_{15}O$	2.07 min	1	1.72

There are two different data acquisition modes in many modern PET systems. One is a two-dimensional (2-D) acquisition with the septa and the other is a three-dimensional (3-D) acquisition without septa. The 2-D acquisition allows only those photons that are emitted parallel to the plane of the detector ring by the septa. In the 3-D acquisition, the inter-plane septa are removed and data are acquired for all possible lines of response. This leads to approximately a fivefold improvement in sensitivity on the 3-D acquisition relative to the 2-D acquisition, but with a considerable increase in random and scatter count rate.

The scattered coincidence event and random coincidence event are the two types of undesirable coincidence events that degrade the PET image quality. The scattered coincidence event occurs when one or both of the γ-rays from an annihilation event outside the coincidence volume of detectors undergo a Compton scatter interaction inside a body. This changes the direction and energy of the γ-ray and results in misidentification of the γ-ray origin. The random coincidence event occurs when annihilation γ-rays from two unrelated positron annihilation events are detected in two opposing detectors within a coincidence timing window of systems. Both the scattered and random

coincidence event produces incorrect positional information and results in a loss of contrast of images by creating a relatively uniform background.

Detector materials and their configuration are important factors in achieving high quality images in the PET systems. The four detector materials that are widely used in PET systems are NaI(Tl), BGO, LSO, and GSO (Table 1.2)[5]. The most important practical feature for scintillation detectors are high mass density and effective atomic number, high light output, and speed. Most commonly used modern PET systems are made with block detectors, which consist of segmented blocks of scintillator coupled to photomultiplier tubes (PMTs). This allows smaller detector elements to be used in improving spatial resolution while reducing the required number of PMTs for detector elements. Many commercial PET systems are arranged in rings or polygonal arrays using the block detectors to achieve high sensitivity.

The most common image reconstruction method adopted in the PET systems is a filtered back projection (FBP) method and ordered subset expectation maximization (OSEM) method. The FBP has been widely used due to its rapid processing time and reliability[6]. However, it may introduce some noise in reconstructed images. Alternatively, the OSEM which is one of iterative

reconstruction methods such as maximum likelihood expectation maximization (MLEM) has been used for the PET systems[6]. This method has several advantages because there is no reconstruction noise and many aspects of the PET system (geometry, scatter, etc) can be considered into the algorithm. Thus, this method can improve signal-to-noise ratio (SNR) and resolution in reconstructed images. On the other hand, these kinds of iterative reconstruction methods have been less often used clinically because of its long reconstruction time. Recently, faster computers have made it possible to for this reconstruction algorithm to be used in clinical situations.

The PET system has many advantages such as imaging of distribution and kinetics of natural and analog biologic tracers and measuring trace amounts of radiopharmaceuticals which represent biological process. They also have an advantage of simultaneously providing the high spatial resolution and high sensitivity. However, the image quality of PET data is degraded by a variety of physical factors including attenuation of photons, detection of scattered and random coincidence photons, finite spatial resolution of PET systems, limited number of counts, and physiologic motion as well as patient motion. While all of these factors limit practical quantitative PET images, the most important

factor that degrades the quality of PET images is the attenuation of photons.

Table 1.2. Scintillating materials and their characteristics for the positron emission tomography.

Name	Density (gm/cm^3)	Effective atomic number, Z_{eff}	Light output (photons per MeV)	Scintillation decay time (nsec)	Scintillation wavelength, λ (nm)	Hygroscopic (Y/N)?
BGO	7.1	75	9,000	300	480	N
GSO	6.7	59	8,000	60	440	N
LSO	7.4	66	30,000	40	420	N
NaI(Tl)	3.7	51	41,000	230	410	Y

2. Attenuation effect and its correction

Photon attenuation is based on the natural property that photons will interact with absorber materials as they pass through those materials[7]. The probability of an interaction occurring depends on the photon's energy and on the

composition and thickness of the absorber. Photon absorption and photon scattering in the absorber are components of general process of the photon attenuation in nuclear medicine.

Photoelectric interaction is an atomic absorption process in which an atom totally absorbs the energy of an incident photon. In Compton interactions, the primary incident photon interacts with loosely bound outer-shell electrons and transfers part of its energy to that electron, which results in scattered photons deflected from the primary direction.

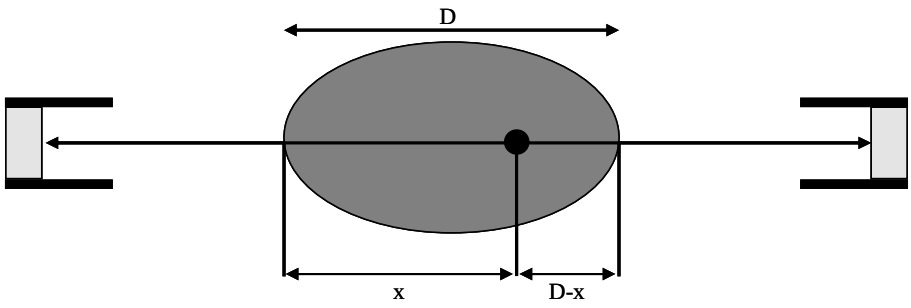

Figure 1.2. Photon attenuation for a given point source. The attenuation is independent of the source position in object for the PET.

Magnitude of the photon attenuation (Fig. 1.2) can be mathematically represented by exponential equation[7]:

$$\begin{aligned} N &= N_0 e^{-\mu x} e^{-\mu(D-x)} \\ &= N_0 e^{-\mu D} \end{aligned} \qquad \text{Eq. 1-2}$$

where N and N_0 are attenuated and un-attenuated count rates (units: counts·s^{-1}), μ is a linear attenuation coefficient (units: cm^{-1}), which represents probability that the photon will undergo an interaction while passing through a unit thickness of absorber, D is a total thickness of the object (units: cm), and x is a location of the source inside the object (units: cm).

The attenuation of photons leads to a loss of quantitative accuracy, lack of image uniformity, and distortions in PET and PET/CT systems[1]. To improve diagnostic accuracy, therefore, correction for attenuation must be done for the PET images in preventing the degradation of the PET image quality[8]. This is accomplished by measuring the attenuation factors using a transmission source such as ^{68}Ge or ^{137}Cs. CT transmission scan in the PET/CT system has been recently introduced for the attenuation correction[9-11].

The Eq. 1-2 can be rewritten to give the attenuation correction factors as shown in Eq. 1-3 and the attenuation correction is achieved by dividing

emission data with the attenuation correction factors.

$$e^{-\mu D} = \frac{N}{N_0} \qquad \text{Eq. 1-3}$$

Practically, the N_0 can be acquired by a blank scan, which is the transmission scan without the object in field of view (FOV). The N can be acquired by the transmission scan with the object in the PET system.

Advantages of attenuation correction are accurate measurement of radioactivity concentrations in body and tumors, preventing a distortion of lesion size, shape, and location, and restoration of intensity for deep lesions[8]. Thus, the attenuation correction is now widely accepted by most of institutions for producing artifact-free, quantitatively accurate data in PET and PET/CT systems.

However, attenuation correction has some limitations, such as additional scan time and radiation exposure, degradation of image quality by a noisy transmission scan and generation of artifacts by a variety of physical factors.

3. Combined PET/CT

Introduction of PET/CT systems, which provides functional and anatomical images to be co-registered inherently because they are acquired close together

in time on a same table and because a relative orientation of the two is known, allows superior matching of images to be obtained[9,10]. This makes it possible to supplement a limited spatial resolution and localization capability of the PET imaging.

Another advantage of the PET/CT system could be shorter acquisition time and superior statistical noise characteristics compared with the conventional method. This is achieved by using the CT transmission scan for attenuation correction, although it needs to be transformed into appropriate attenuation coefficients at 511 keV emission energy to calculate for the attenuation factors from the CT image[9].

The CT has a spectrum of photons from 40 keV to 140 keV, while the PET attenuation measurements use mono-energetic 511 keV annihilation photons. Thus, most of commercial PET/CT systems adopt a scaling method using effective x-ray energy in the range of 50-80 keV for the energy transformation [9]. The energy scaling can be simply achieved by using an equation 1-4[1], when all image regions are air, water, and a combination of air and water.

$$\mu_{511} = \frac{\mu_{511,water}}{\mu_{x-ray,water}} \mu_{x-ray} \qquad \text{Eq. 1-4}$$

where μ_{511} is the adjusted values for 511 keV, $\frac{\mu_{511,water}}{\mu_{x-ray,water}}$ is the ratio of attenuation coefficient of water, and μ_{x-ray} is the attenuation coefficient of x-ray CT.

However, the scaling method can lead to poor approximation when photoelectric contributions dominate at the CT energies, especially for materials with higher atomic Z values. Thus, it has been known that insufficient energy transformation can generate inappropriate uptake on the PET images by the CT-based attenuation correction.[12-29].

Another approach for CT-based attenuation correction is a segmentation method that forms attenuation images at 511 keV by segmenting the reconstructed CT image into different tissue types (typically, soft tissue, bone, and lung). The problem with this method is an inaccurate representation by a discrete set of segmented values in the some soft tissue regions such as a lung, which has a continuous variation of density.

To overcome the problems inherent to scaling and segmentation methods, a hybrid method which has a combination of scaling and segmentation methods is proposed by Kinahan et al[9]. To estimate the attenuation image at 511 keV by this method, a threshold is used to separate out the bone component of the CT

image, and then separate scaling factors is used for the bone and non-bone component.

4. Attenuation correction artifacts

Attenuation correction can produce artifacts by a variety of factors including patient motion, metallic prosthesis, contrast agent, and respiratory motion in PET and PET/CT images[12-26, 30, 31].

Patient motion between emission and transmission scans can lead to some serious artifacts by misregistration when the attenuation correction is performed[8,15].

High density objects such as the metallic prosthesis can cause artifacts in the PET and PET/CT images because of high density difference between the metallic materials and surrounding materials resulting in an inaccurate estimation of attenuation coefficients[12-19].

Contrast agents are generally adopted to delineate anatomical structures in diagnostic CT scanning[26]. Intravenous contrast agents are required for delineation of vascular structures and parenchymal alteration. Oral contrast agents are usually administered for delineation of intestinal structures in

abdomen. The CT-based attenuation correction in the commercial PET/CT systems typically doesn't consider the contrast agent, when they translate the x-ray energy to 511 keV γ-ray energy. Thus, it may generate artifacts in the attenuation-corrected PET images[20-26].

Respiratory motion is also one of the factors which can introduce artifacts because of differences in respiratory status between the PET and CT scanning[30, 31].

Many of the previously stated physical factors can degrade image quality and produce artifacts in the PET and PET/CT images. Thus, it is very important to understand these kinds of artifacts to prevent misinterpretation during diagnosis or quantitative analysis.

5. Research objectives

The purpose of this dissertation was to study the impact of metallic materials and contrast agents in PET and PET/CT images.

Simulation and experiments were performed to study the severity of artifacts from the metallic materials. A variety of factors were evaluated including size of the metallic materials, noise component, spatial resolution, motion between

emission and transmission scan, reconstruction algorithm, and density of the metallic materials.

Simulation and experiments were also carried out to study the impact of contrast agent. A variety of factors were evaluated including non-uniform enhancement of contrast agent, concentration and distribution size for that non-uniform enhancement, noise component, spatial resolution, reconstruction algorithm, image quality for with and without contrast agent, hypo-attenuation of contrast agent, and different time phases for contrast agent.

II. IMPACT OF METALLIC MATERIALS FOR ATTENUATION CORRECTION

1. Simulation

A. Generation of emission and transmission maps

Mathematical emission and transmission density maps with oval cross-section of 36 cm × 21 cm were made to simulate whole body FDG imaging. A 50 cm diameter was used for FOV and transaxial slice was binned into a 128 × 128 pixel array (≈ 3.9 mm per pixel). The emission map was assigned a uniform activity and the transmission map was generated with a linear attenuation coefficient (0.093/cm)[10] per pixel of water for 511 keV. Aluminum and titanium of 4 mm and 20 mm diameter were introduced with a linear attenuation coefficient (0.224/cm and 0.363/cm)[32] per pixel for 511 keV at body edge and internally on the transmission map. The transmission map introduced aluminum and titanium was shifted by 2, 4, 8, 12, and 20 mm horizontally. Figure 2.1 shows the simulation procedures for the metallic materials.

B. Sinogram

PET projection data for all possible combinations of detector pairs in a given ring are conventionally stored in the form of sinograms[1]. Each element in the sinogram represents the sum of all the activity along the line joining the two detectors. Each row in the sinogram matrix represents the projected activity of parallel detector pairs at a given angle relative to the detector ring.

In this study, all of the projection data were generated with 336 numbers of projection angles and a 128 × 128 matrix size. Attenuated projections for the emission map were produced by dividing emission projections with a non-shifted transmission projection data.

C. Noise and Gaussian smoothing

A variety of noise values were applied to the attenuated emission projection data with a Poisson distribution as shown in Eq. 2-1[2].

$$P(N;m) = e^{-m} m^{N} / N! \quad \text{for } N = 0, 1, 2, \cdots \qquad \text{Eq. 2-1}$$

where m is a shape parameter which indicates average number of events. For realistic features, mean total count measured from eleven whole body PET projection data were used to determine the noise level.

Gaussian smoothing makes an image blurry and degree of smoothing is determined by standard deviation (σ) of the Gaussian. The 2-D Gaussian smoothing has a form as shown in Eq. 2-2[2]:

$$G(x, y) = e^{-(x^2+y^2)/2\sigma^2} \qquad \text{Eq. 2-2}$$

where x and y represent a distance from a centered in arbitrary pixel position. To simulate a whole body PET image resolution in the general PET systems, the Gaussian smoothing with 6, 8, and 10 mm was applied to the emission and transmission projection data.

D. Attenuation correction and image reconstruction

Attenuation correction was done by multiplying attenuated emission projections with all the transmission projections. Attenuation-corrected images were reconstructed with FBP and OSEM.

E. Data analysis

All reconstructed images were evaluated using visual analysis. Activity profiles were measured for artifacts, along with their intensities. Standard deviation and coefficient of variation were used to assess image quality. The

standard deviation was calculated by using Eq. 2-3:

$$SD = \sqrt{\frac{n\sum x^2 - (\sum x)^2}{n(n-1)}} \qquad \text{Eq. 2-3}$$

where n is a number of measurement and x is a mean value of measured data.

The coefficient of variation was calculated by using Eq. 2-4:

$$CV(\%) = \frac{SD}{Mean}100 \qquad \text{Eq. 2-4}$$

Table 2.1 describes variables evaluated in the simulation.

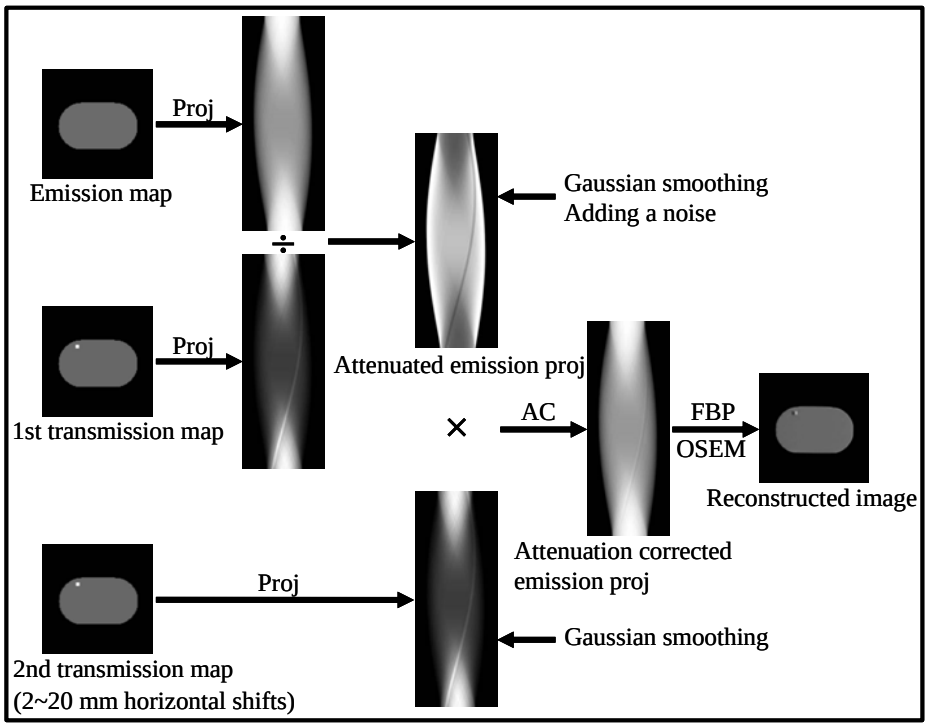

Figure 2.1. Schematic diagram of the simulation procedure for the aluminum and titanium (Proj: projection, AC: attenuation correction).

Table 2.1. Variables evaluated in the simulation.

Study no.	Variables
1	Size (4 & 20 mm diameter)
2	Density (aluminum vs. titanium)
3	Noise level
4	Resolution (6, 8, 10 mm Gaussian smoothing)
5	Phantom movement (2~20 mm horizontal shifts between emission and transmission scanning)
6	Reconstruction algorithm (FBP vs. OSEM)

2. Experiments

A. Phantom preparation

A whole body phantom is 40 cm long with an oval cross-section of 36 cm × 21 cm and a fillable volume of 25 liters (Fig. 2.2). The whole body phantom was prepared with various aluminum shapes of 3, 5, and 8 mm thick inserts and titanium rod of 3, 5, 6, 10, and 13 mm thick inserts. F-18 background concentration of 10 kBq/ml (aluminum) and 8 kBq/ml (titanium) was used for

the whole body phantom.

B. Data acquisition

GE Advance PET and GE Discovery ST PET/CT systems (GE Medical Systems, Milwaukee, WI, USA) were used for data acquisition. The PET system consists of 4.0 mm × 8.1 mm × 30 mm BGO scintillator elements in 6 × 6 blocks with two dual photomultiplier tubes (PMTs) per block. Eighteen rings of 92.7 cm diameter form a 15.2 cm axial FOV. Retractable tungsten septa of 117 mm long and 1 mm thick are equipped for 2-D and 3-D data acquisition. The PET/CT system consists of 6.3 mm × 6.3 mm × 30 mm BGO scintillator elements in 6 × 6 blocks with a single quad cathode PMTs per block. Four rings of 89 cm diameter form a 15.7 cm axial FOV. Retractable tungsten septa of 54 mm long and 0.8 mm thick are equipped for 2-D and 3-D data acquisition.

The whole body phantom was imaged using both the PET and PET/CT systems. On the PET, 4 and 20 min emission scans and 2.5 and 10 min ^{68}Ge transmission scans were performed. On the PET/CT, 4 and 20 min emission scans and high-resolution 140 kVp CT were acquired. Transmission data were

acquired with 0, 2, 4, and 8 mm horizontal shifts between the phantom emission and transmission position.

C. Attenuation correction and image reconstruction

The acquired images were corrected for attenuation and reconstructed with FBP and OSEM. All the transmission scans for both the PET and PET/CT were used for attenuation correction. Hanning filter with a cutoff frequency of 0.85 cycles/cm was used for the FBP reconstruction. Twenty eight and thirty subsets, and two iterations were used for the OSEM reconstruction in the PET and PET/CT. Segmented attenuation correction (SAC) and measured attenuation correction (MAC) methods were tested for the ^{68}Ge transmission.

D. Data analysis

All of the reconstructed images were evaluated using visual analysis. Activity profiles were measured for artifacts, along with their intensities. The standard deviation and coefficient of variation were used to assess image quality. Table 2.2 describes the variables evaluated in the experiments.

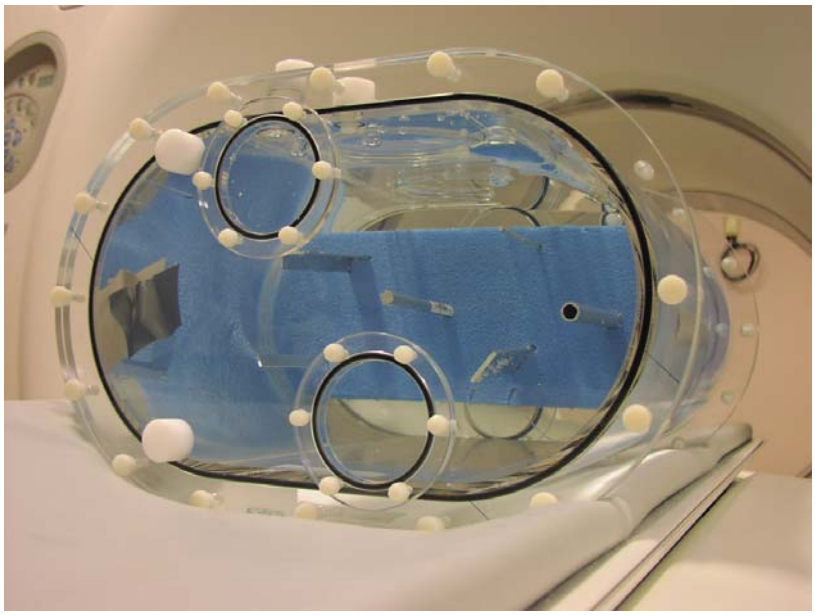

Aluminum inserts

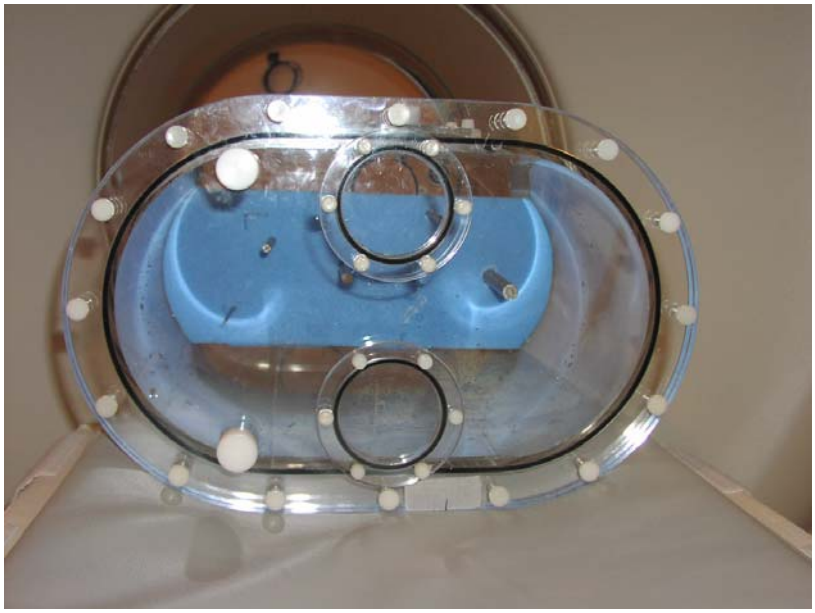

Titanium inserts

Figure 2.2. Whole body phantom with aluminum and titanium inserts.

Table 2.2. Variables evaluated in the experiments.

Study no.	Variables
1	Shape
2	Thickness
3	Density (aluminum vs. titanium)
4	Acquisition duration (emission 4 min/ transmission 2.5 min vs. emission 20 min/transmission 10 min)
5	^{68}Ge-based attenuation correction vs. CT-based attenuation correction
6	Phantom movement (0, 2, 4, 8 mm horizontal shifts between emission and transmission scanning)
7	Reconstruction algorithm (FBP vs. OSEM)
8	Attenuation correction method (MAC vs. SAC)

III. IMPACT OF CONTRAST AGENTS FOR ATTENUATION CORRECTION

1. Experiments

A. Phantom preparation

A whole body phantom was prepared with iodine-based contrast agents of various concentrations of 0% (water), 1%, 3% (clinical concentration for oral contrast agent), 5%, 10%, 20%, and 100% (clinical concentration for intravenous contrast agent). Background area of the whole body phantom was filled with and without water. Figure 3.1 shows the whole body phantom with contrast agent filled with various concentrations.

B. Data acquisition and image reconstruction

Transmission scan was acquired with CT in PET/CT system. Different voltage values of 120 kVp and 140 kVp were tested for the CT transmission scan. The acquired images were reconstructed with FBP.

C. Data analysis

Relationship between Hounsfield Unit and the concentration of contrast agents and the tube voltage was assessed. Table 3.1 describes variables evaluated in the experiments.

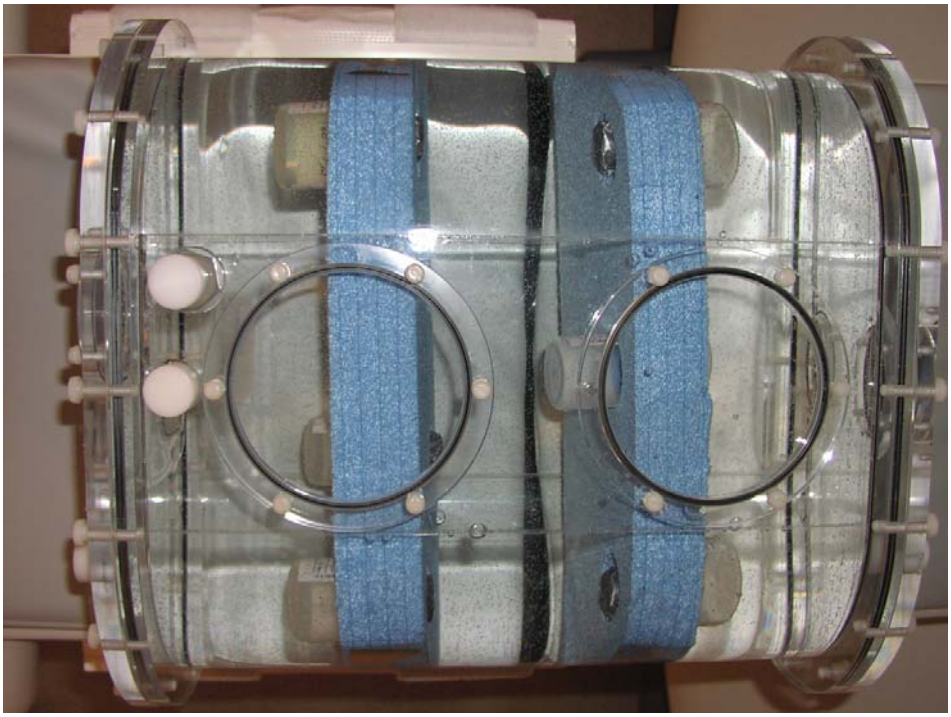

Figure 3.1. Whole body phantom with iodine-based contrast agents filled with various concentrations.

Table 3.1. Variables evaluated in the experiments.

Study no	Variables
1	Concentration (0, 1, 3, 5, 10, 20, 100%)
2	Tube voltage (120 kVp vs. 140 kVp)

2. Simulation

A. Generation of emission and transmission maps

Non-uniform enhancement of contrast agent

Contrast agents can be enhanced non-uniformly in body and this non-uniform enhancement of contrast agents can affect image quality on CT-based attenuation-corrected PET images.

The emission and transmission maps that were generated for the simulation of metallic materials were used to study the effects of non-uniform enhancement of contrast agents. A liver was introduced on the emission and transmission maps. The liver on the emission map was assigned with a uniform activity to have threefold activity of background area. Mean count values measured from nine patients for normal liver and normal background tissue were used to determine the ratio between liver and background area. Linear attenuation coefficient $(0.164/cm)^{32}$ per pixel of iodine for 511 keV was assigned to the liver on the transmission map to simulate the presence of contrast agent. Three circular-shapes of hyper-attenuated areas were then generated on the liver to mimic the non-uniform enhancement. Hyper-attenuated areas of different sizes of 1.2 cm, 1.6 cm, and 2.4 cm were tested for

the non-uniform enhancement of contrast agent. Different concentrations of contrast agent of 20%, 40%, and 60% increased for the liver activity were also tested for the non-uniform enhancement of contrast agent. Figure 3.2 shows the simulation procedure for the non-uniform enhancement of contrast agent.

Tumor detection in presence of contrast agent

Presence of contrast agent can affect image quality and tumor detection on CT-based attenuation-corrected PET images.

The emission and transmission maps that were generated for the simulation of metallic materials were used to study the effect of contrast agent for the image quality and tumor detection. The liver that was made for the simulation of non-uniform enhancement of contrast agent was introduced on the emission and transmission maps. Three circular-shapes of tumors were introduced on the liver for the emission map and different sizes of 1.2 cm, 1.6 cm, and 2.4 cm were tested for those tumors, respectively. The tumors were assigned with a 100% increased activity for the liver activity. The liver on the transmission map was assigned with a linear attenuation coefficient per pixel of iodine for 511 keV to simulate the presence of contrast agent.

Hypo-attenuation of contrast agent

Enhancement of contrast agents in tumors depends on the tumor types, hyper-attenuating or hypo-attenuating[33]. The tumors typically have a high FDG uptake on PET emission images, but contrast agents can be hypo-attenuated in the tumors on CT transmission images. Therefore, hypo-attenuated contrast agent can affect the intensity of the tumors on the CT-based attenuation-corrected PET images.

The same emission and transmission maps for the simulation of metallic materials were used to study the effect of hypo-attenuation of contrast agent. The same liver for the simulation of non-uniform enhancement of contrast agent was introduced on the emission and transmission maps. Three different sizes (1.2 cm, 1.6 cm, and 2.4 cm) of circular-shaped tumors were introduced on the liver for the emission and transmission maps. The tumors on the transmission map were assigned with a linear attenuation coefficient per pixel of water for 511 keV, which is a lower value than what the iodine had, to simulate the hypo-attenuation. A variety of tumor densities (10%, 20%, 50%, 100%, and 200% increased for the liver activity) was tested on the emission map. In addition, different time phases were studied for the distribution of

contrast agent on the liver changing by ± 20% and ± 40% of the linear attenuation coefficient for the liver on the transmission map. Figure 3.3 shows the simulation procedure for the hypo-attenuation of contrast agent.

B. Sinogram

All projection data were generated with 336 numbers of projection angle and 128 × 128 matrix size. Attenuated projections for the emission map were produced by dividing emission projections with a uniform transmission projection data.

C. Noise and Gaussian smoothing

The same noise values that were used for the simulation of metallic materials were applied to the attenuated emission projection data with the Poisson distribution. The same Gaussian smoothing values for the simulation of metallic materials were also applied to the emission and transmission projection data.

D. Attenuation correction and image reconstruction

Attenuation correction was done with all transmission projections with the non-uniform distributed contrast agent for the emission projection with a normal liver. Attenuation correction was done with transmission projections with and without a distribution of contrast agent on the liver for the emission projection with tumors on the liver. Attenuation correction was done with all transmission projections with hypo-attenuation in tumors for emission projections with the tumors on the liver. Attenuation-corrected images were reconstructed by FBP and OSEM.

E. Data analysis

All reconstructed images were evaluated using visual analysis. The coefficient of variation and signal to noise ratio (SNR) were calculated to assess the image quality using Eq. 2-3 and Eq. 3-1.

$$SNR = \frac{C_{tumor} - \overline{C}_{bkg}}{SD_{bkg}} \qquad \text{Eq. 3-1}$$

where C_{tumor} is a measured count for tumors, $\overline{C}_{bkg}$ is a mean measured count for background, SD_{bkg} is a standard deviation for background. Table

3.2 describes variables evaluated in the simulation.

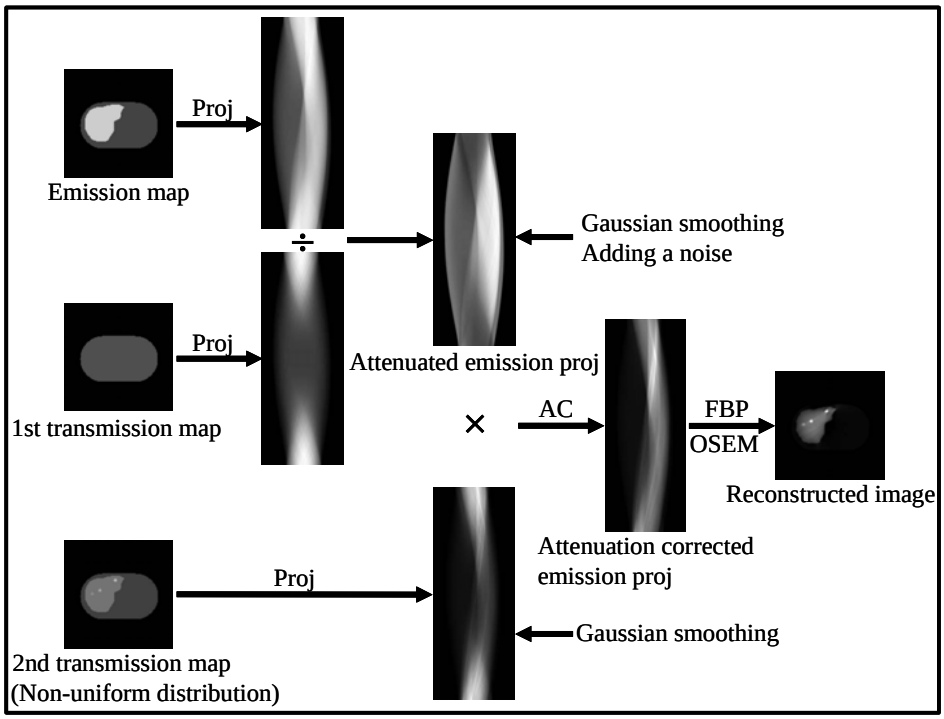

Figure 3.2. Schematic diagram of the simulation procedure for the non-uniform enhancement of contrast agent on the liver (Proj: projection, AC: attenuation correction).

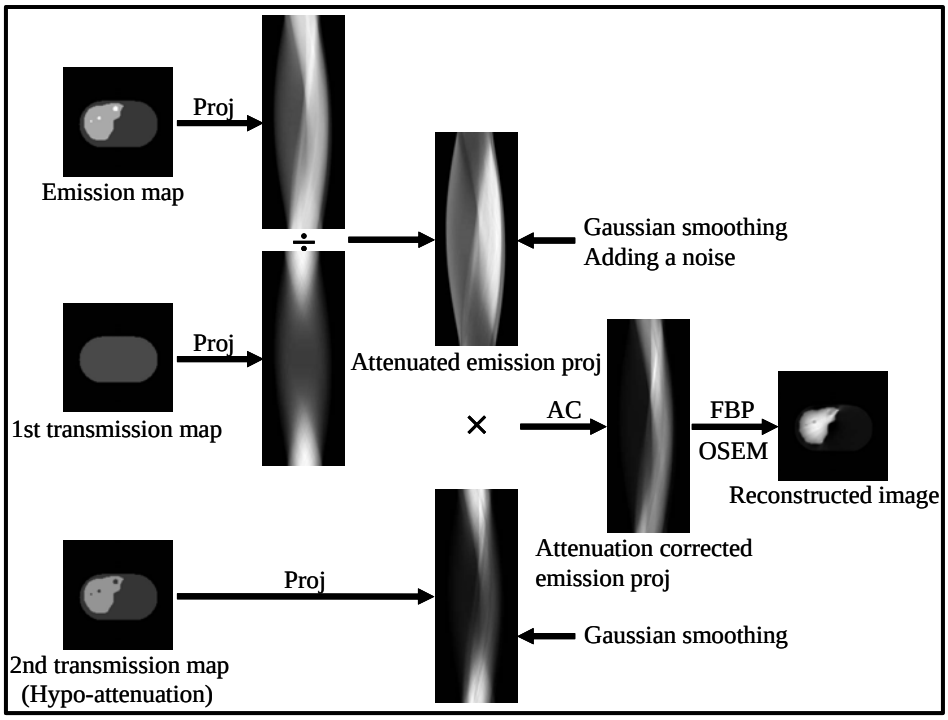

Figure 3.3. Schematic diagram of the simulation procedure for the hypo-attenuation of contrast agent in the tumor (Proj: projection, AC: attenuation correction).

Table 3.2. Variables evaluated in the simulation.

Study no.	Variables
1	Non-uniform enhancement of contrast agent
2	Concentration
3	Size of non-uniformly enhanced contrast agent
4	Noise level
5	Resolution (6, 8, 10 mm Gaussian smoothing)
6	Reconstruction algorithm (FBP vs. OSEM)
7	Hypo-attenuation of contrast agent in tumor

IV. RESULTS *METALLIC MATERIALS*

1. Simulation studies

During the interval between emission and transmission acquisition, aluminum and titanium structures with body motion introduced substantial hyper- and hypo-uptake compared with background uptake.

Artifacts generated by the metallic materials were not affected by the position of the metallic materials.

Small object of 4 mm in diameter generated no artifacts at low count rates and small shifts of transmission data (Fig. 4.1). In high count rates, the small object produced artifacts with large shifts. However, no observable effects were produced on images with small shifts that were under the high count rates. Large object of 20 mm in diameter showed artifacts under a relatively lower count rate than did small object, even those with small shifts. The aluminum object of 20 mm in diameter with small shifts showed both an artifact and high intensity values through this artifact. However, no artifact was observed for small object of 4 mm in diameter with small shifts, resulting in no remarkable intensity profile.

Noise level can also affect the impact of aluminum and titanium. Less evidence of the artifact in the visibility can result as the count rate decreases (Fig. 4.2).

Density of the metallic materials also affects any generation of artifacts. Figure 4.3 shows that the more dense titanium produced stronger artifacts than aluminum, as demonstrated by the intensity profile through the artifact. The more dense titanium produced an artifact even at lower count rates and smaller shifts than aluminum.

Poor image resolution reduced the impact of metallic materials, especially those with small size and shifts. Artifacts generated by the aluminum and titanium were blurred by Gaussian smoothing. These artifacts were even less evident in 10 mm Gaussian smoothing for small object and small shifts (Fig. 4.4). The maximum intensity values through the artifacts were decreased by the smoothing (Table 4.1).

Movement between the emission and transmission maps produced hyper- and hypo-uptake caused by the metallic materials. A strong increase of an artifact and its intensity was observed as movement between emission and transmission maps increased horizontally (Fig. 4.5). The standard deviation

values were increased as the movement is increased (Table 4.2).

The image reconstructed by the OSEM was relatively less noisy than that produced using the FBP (Fig. 4.6) and has a superior coefficient of variation of 9.05% than the FBP does at 9.50% (Table 4.3). But there was no visual difference in recognizing the artifact between both images.

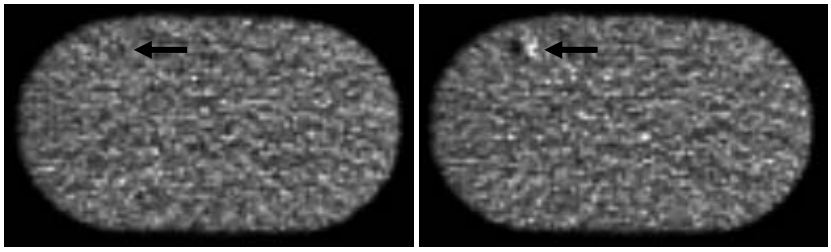

4 mm diameter 20 mm diameter

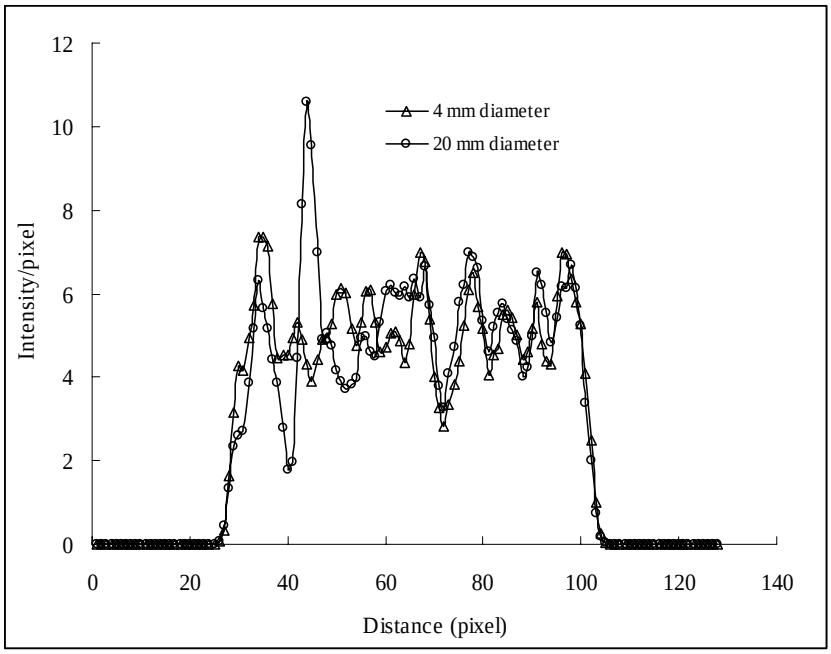

Figure 4.1. Emission images and their intensity profiles for the aluminum of 4 mm and 20 mm diameters. The aluminum object of 20 mm in diameter with small shifts showed both an artifact and high intensity values through this artifact. However, no artifact was observed for small object of 4 mm in diameter with small shifts, resulting in no remarkable intensity profile.

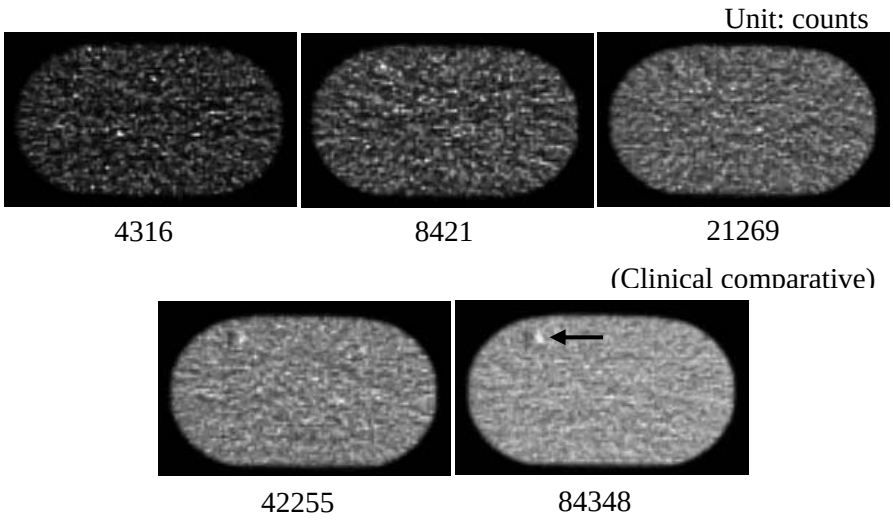

Figure 4.2. Emission images for a variety of noise values. Impact of the metallic materials is affected by the noise level, resulting in less evidence of the artifact as the count rate decreases.

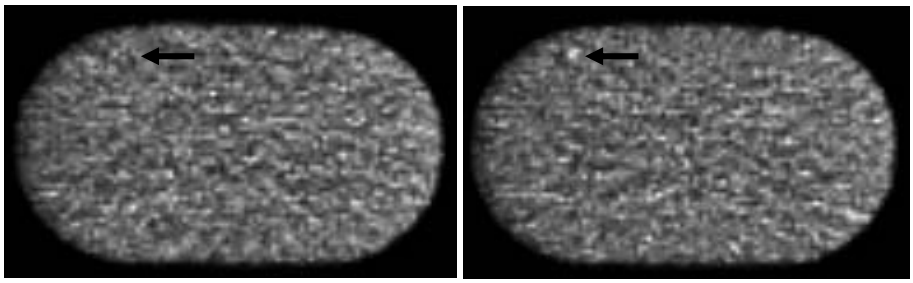

Aluminum Titanium

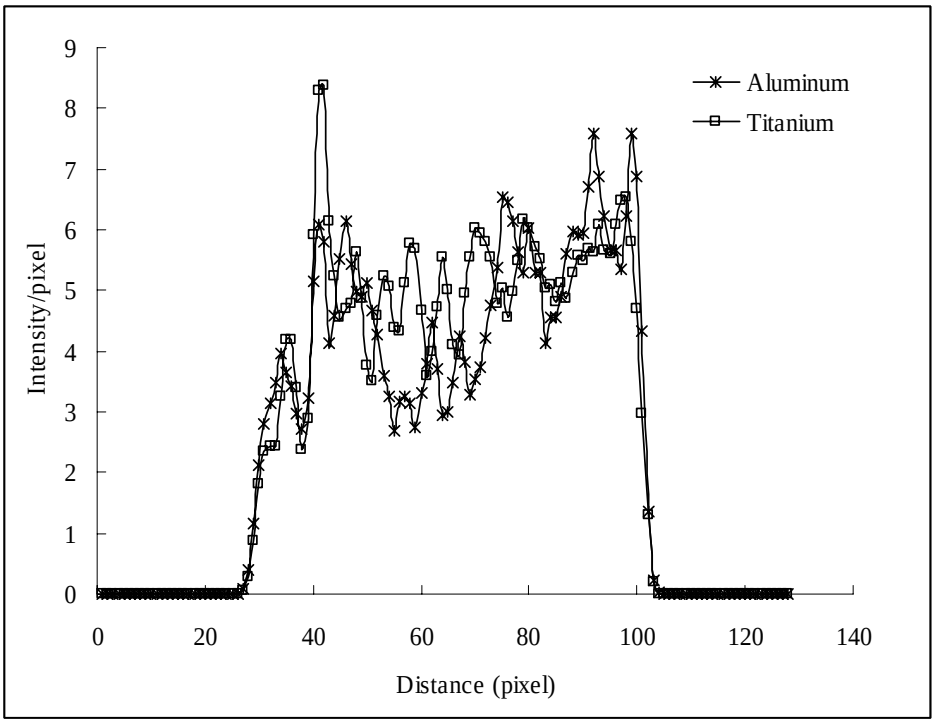

Figure 4.3. Emission images and their intensity profiles for the aluminum and titanium of 4 mm in diameter. The more dense titanium produced a stronger artifact than did the aluminum, as demonstrated by the intensity profile through the artifact.

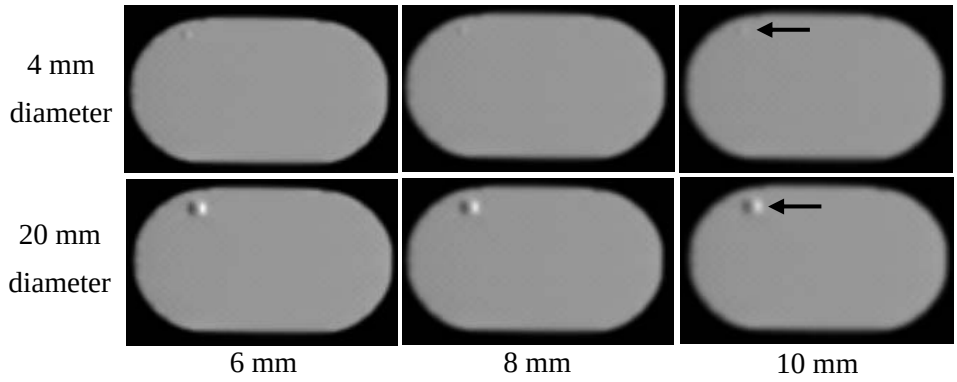

Figure 4.4. Emission images with Gaussian smoothing of 6, 8, and 10 mm without noise component. Artifact introduced by the metallic materials was less evident in the 10 mm than the 6 mm or 8 mm Gaussian smoothing.

Table 4.1. Maximum intensity values in the artifacts for the each values of Gaussian smoothing. The poor resolution reduced the intensity value of artifact.

	Maximum intensity values	
Values of Gaussian smoothing	4 mm diameter	20 mm diameter
6 mm	1.23	2.47
8 mm	1.14	2.13
10 mm	1.07	1.87

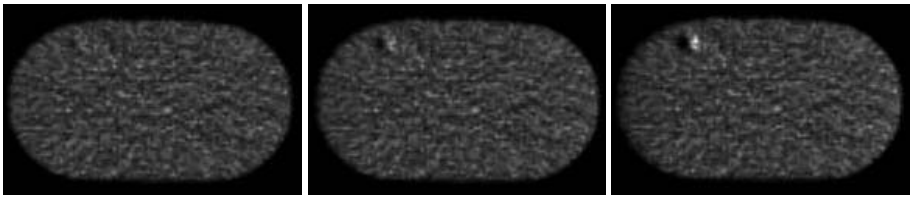

2 mm shift 4 mm shift 8 mm shift

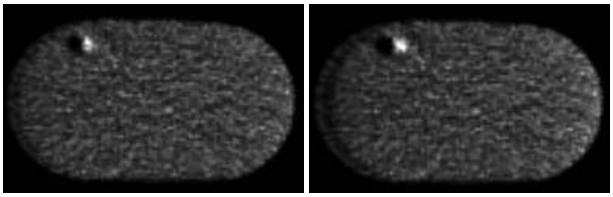

12 mm shift 20 mm shift

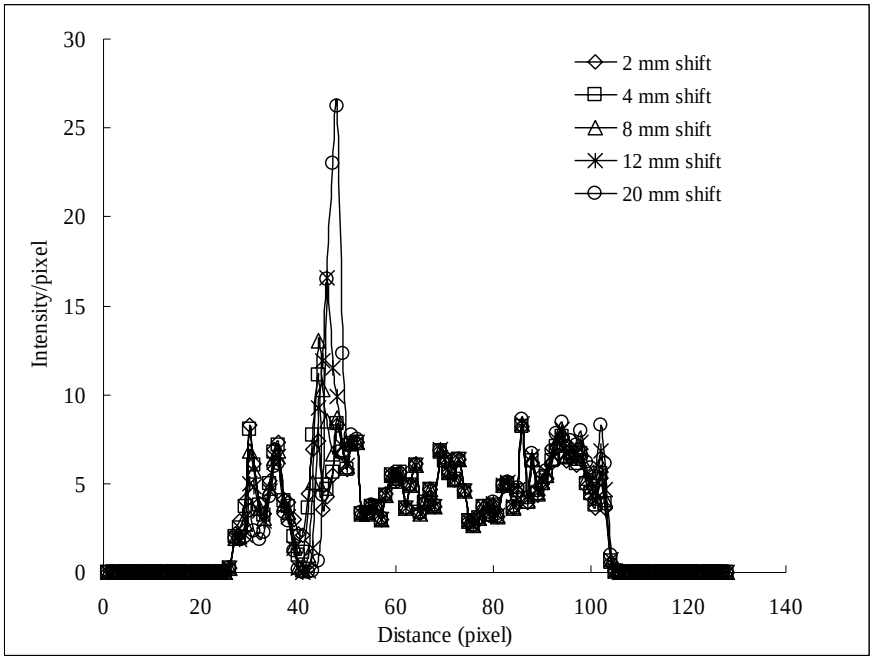

Figure 4.5. Emission images and their intensity profiles for various shifts between emission and transmission maps. A strong increase of an artifact was observed as movement between emission and transmission maps increased horizontally.

Table 4.2. Standard deviation for the images with movement between emission and transmission maps. The standard deviation values were increased, as the movement is increased.

Movement	SD
2 mm shift	0.45
4 mm shift	0.47
8 mm shift	0.52
12 mm shift	0.58
20 mm shift	0.61

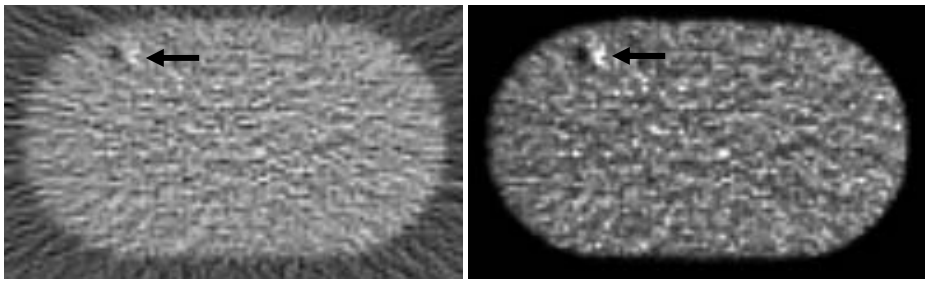

FBP OSEM

Figure 4. 6. Emission images reconstructed by FBP and OSEM. The image reconstructed by the OSEM was relatively less noisy than the FBP, but there was no visual difference in recognizing the artifact between both images.

Table 4.3. Coefficient of variation for the images reconstructed by FBP and OSEM. The OSEM has a superior coefficient variation values than the FBP, although there is no much difference between the two values.

	CV (%)
FBP	9.50
OSEM	9.05

2. Experimental studies

Artifacts were observed in the result images that resembled those simulated by aluminum and titanium structures with body motion.

It was less evident that the generation of artifacts is affected by the shape of the metallic materials.

However, the size of the metallic materials was an important factor in producing artifacts. Larger aluminum and titanium materials introduced relatively strong artifacts into the visibility at shorter acquisition durations and smaller shifts.

The more dense titanium produced stronger artifacts at lower count densities and smaller shifts than did aluminum (Fig. 4.7).

At clinical acquisition duration without movement, aluminum had no inappropriate hyper-uptake for all sizes. Artifacts were also less evident with movement at clinical acquisition duration. High count studies revealed artifacts for larger structures (≥ 5 mm) with movement. Figure 4.8 shows that for aluminum, artifacts appeared at longer acquisition duration, but not at shorter acquisition duration. For titanium, artifacts were seen in larger sizes (≥ 10 mm) at clinical acquisition duration, although there was no movement between

the emission and transmission scans. At high-count studies, hyper-uptake without movement was observed adjacent to titanium over the 6 mm thickness. With movement, artifacts were introduced over the 5 mm thickness at high-count studies.

There was no visual difference between artifacts generated by ^{68}Ge-based attenuation correction and CT-based attenuation correction, although the CT-based attenuation-corrected images were blurred more than those that were ^{68}Ge-based, resulting in less evident artifacts (Fig. 4.9).

Movement between emission and transmission scans produced a strong increase of artifacts on the images, and the intensity profile revealed a dramatic increase of intensity values throughout the artifact (Fig. 4.10). The standard deviation values were increased, when the movement is increased (Table 4.4).

There was no visual difference to observe in the artifacts between FBP and OSEM, although the OSEM was relatively less noisy than the FBP like the simulation (Fig. 4.11). The image reconstructed by the OSEM has a superior coefficient of variation of 9.21% than the FBP does at 11.73% (Table 4.5).

The images corrected by the MAC and SAC methods for attenuation showed slightly different aspects in artifacts (Fig. 4.12), while less evidence in artifacts

were seen in images corrected by the SAC method than those corrected using the MAC method. The intensity profile also showed a lower intensity values through the artifact in the images corrected by the MAC method than the images corrected by the SAC method.

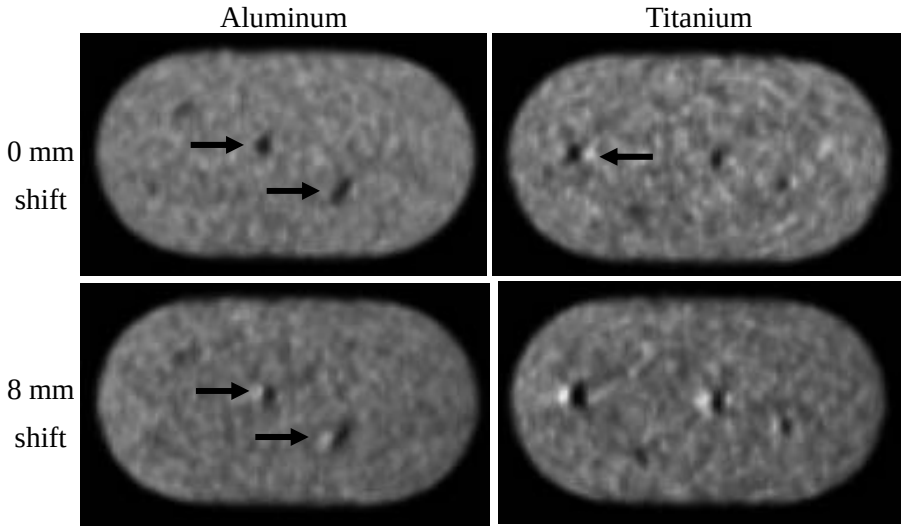

Figure 4.7. Whole body phantom images with aluminum and titanium inserts shifted by 0 mm and 8 mm between emission and transmission scans. The more dense titanium produced stronger artifacts than aluminum did, both with and without movement.

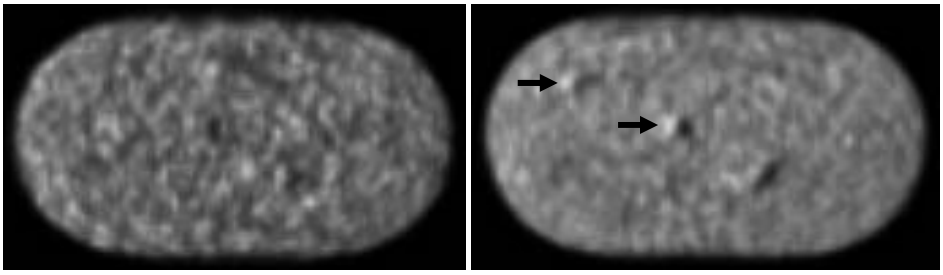

Emission 4 min/
Transmission 2.5 min

Emission 20 min/
Transmission 10 min

Figure 4.8. Whole body phantom images with aluminum inserts for emission 4 min/transmission 2.5 min, and emission 20 min/transmission 10 min shifted by 8 mm horizontally between the emission and transmission scans. Artifacts appeared at longer acquisition durations, but not at shorter acquisition durations.

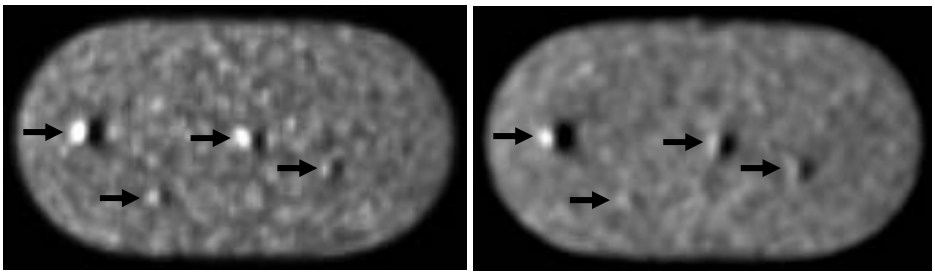

^{68}Ge-based CT-based

Figure 4.9. Whole body phantom images with titanium inserts corrected for attenuation by ^{68}Ge-based and CT-based methods. There was no visual difference between the ^{68}Ge-based and the CT-based attenuation corrections regarding the introduction of artifacts. But the CT-based attenuation-corrected images were blurred more than the ^{68}Ge-based attenuation-corrected images, which resulted in less evident artifacts.

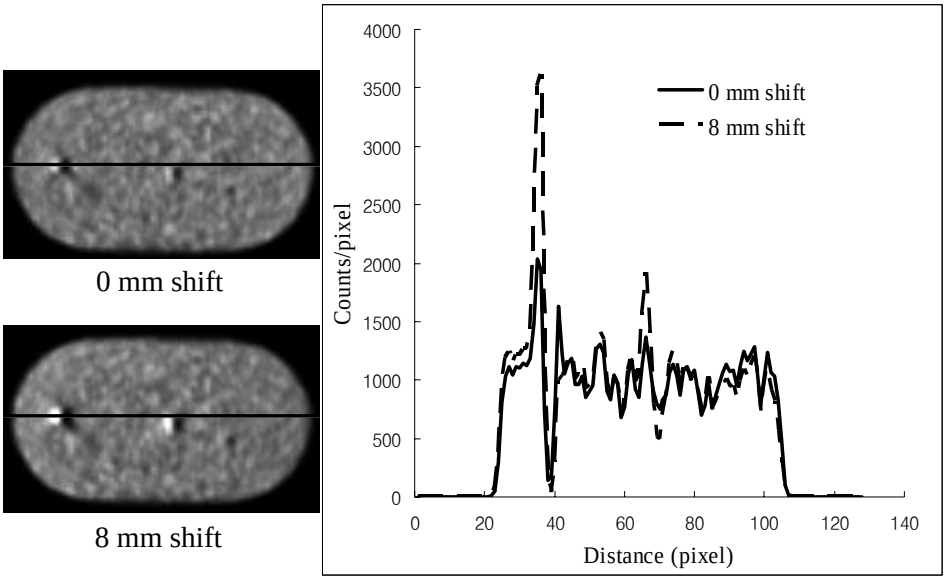

Figure 4.10. Whole body phantom images with titanium inserts and their intensity profiles through the artifact shifted by 0 mm and 8 mm horizontally between the emission and transmission scans. Hyper-uptake adjacent to the titanium with shift is more remarkable than the no shift image, although it still showed hyper-uptake near the titanium without shift.

Table 4.4. Standard deviation for the images with movement between emission and transmission scans. The standard deviation values are increased, when the movement between emission and transmission scan is increased like the simulation.

Movement	SD
0 mm shift	48.28
2 mm shift	48.59
4 mm shift	49.67
8 mm shift	50.26

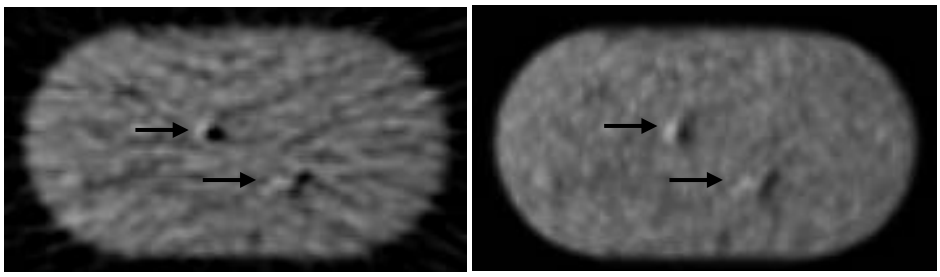

FBP OSEM

Figure 4.11. Whole body phantom images with aluminum inserts reconstructed by FBP and OSEM. Similar with the simulation, there was no visual difference in artifacts between the OSEM and FBP, although the OSEM was relatively less noisy than the FBP.

Table 4.5. Coefficient of variation values for the images reconstructed by FBP and OSEM. The OSEM has a superior coefficient of variation values than the FBP like the simulation.

	CV (%)
FBP	11.73
OSEM	9.21

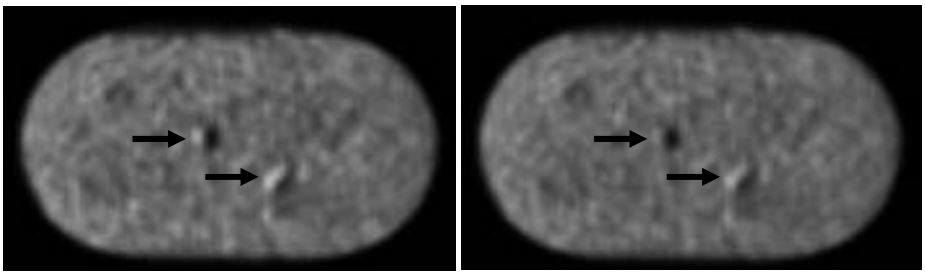

MAC SAC

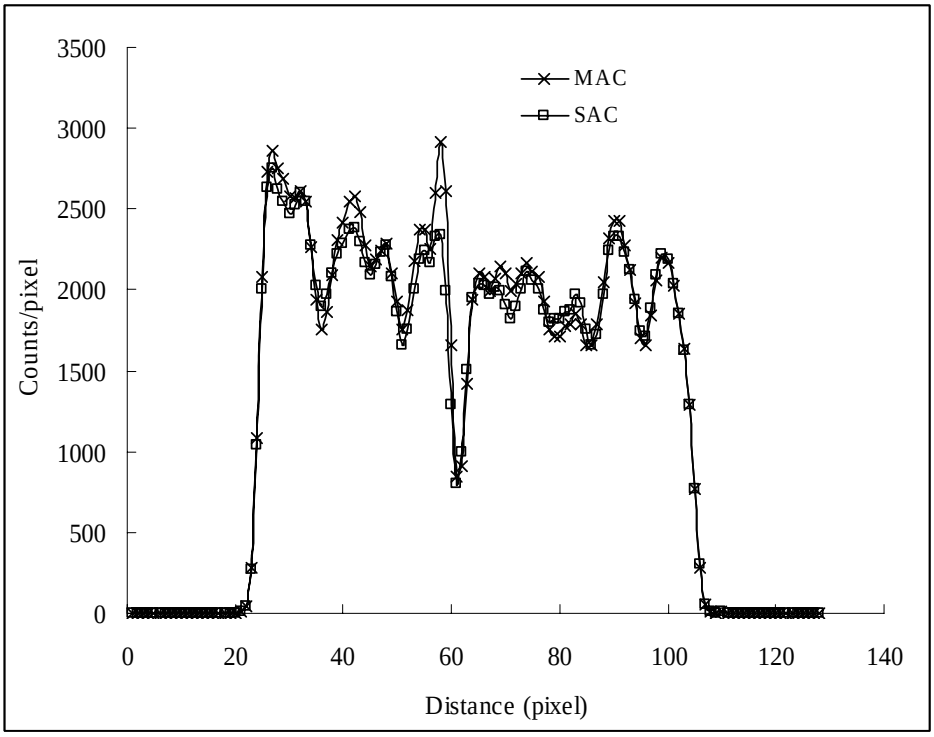

Figure 4.12. Whole body phantom images with aluminum inserts corrected by the MAC and SAC methods for attenuation. The images corrected by the SAC method showed less evidence of artifacts and a lower intensity values through the artifact than those corrected by the MAC method.

V. RESULTS *CONTRAST AGENT*

1. Experimental studies

Experimental studies showed that Hounsfield Unit is increased as the concentration of contrast agent is increased. The Hounsfield Unit was higher at 120 kVp than 140 kVp for both air and water, when the concentration of contrast agent was the same (Fig. 5.1).

2. Simulation studies

Simulated non-uniform enhancement of contrast agent on the liver in transmission map produced inappropriate hyper-uptake on the attenuation-corrected emission images (Fig. 5.2).

The artifacts introduced by the non-uniform enhancement are influenced by the concentration and size of non-uniformly distributed contrast agent. The non-uniform enhancement of 1.2 cm in diameter introduced less evident artifacts compared to the larger 1.6 cm and 2.4 cm sized enhancements. The more dense concentration of contrast agent that was increased by 60% for the linear attenuation coefficient per pixel of liver introduced stronger artifacts

than the 20% and 40% increased agents did. Higher signal-to-noise ratio values were acquired for the artifacts, when concentration and size were increased for the non-uniformly enhanced contrast agent (Table 5.1).

High noise component degraded the impact of non-uniformly enhanced contrast agents. Figure 5.3 shows that artifacts caused by the non-uniform enhancement of contrast agent are less evident as the count rate decreases.

The impact of non-uniform enhancement of contrast agent is reduced by poor image resolution (Fig. 5.4). The artifacts generated by non-uniform enhancement of contrast agent were less evident in the 10 mm than the 6 mm or 8 mm Gaussian smoothing, especially for the smaller sized and lower concentration of non-uniformly enhanced contrast agent. The maximum intensity values in the artifacts were also decreased by smoothing (Table 5.2).

There was no observable visual difference in artifacts between FBP and OSEM (Fig. 5.5), although the image reconstructed by the OSEM has a superior coefficient of variation of 13.59% than the FBP does at 15.11% (Table 5.3).

Image quality and tumor detection is affected by the presence of contrast agent on the liver. Images corrected for attenuation without contrast agent on

the transmission map have a superior coefficient of variation value of 9.34% than the images corrected for attenuation with contrast agent does at 10.74%. The images corrected for attenuation without contrast agent on the transmission map also have a superior signal to noise ratio value between tumors and background area (Table 5.4) than the images corrected for attenuation with contrast agent.

Hypo-attenuated contrast agent in tumors on the transmission map reduced the tumor intensity on the attenuation-corrected emission images (Fig. 5.6). The degree of reduction of the tumor intensity depends on the tumor density in the emission map. In our simulation, the tumors were not observable by the hypo-attenuation of contrast agent, when the tumor density was increased by 100 % for the liver density. The values of tumor density which make the tumors invisible on the emission images by the hypo-attenuation is influenced by the different time phase (Fig. 5.7). For example, compared to the situation where the value of the tumor density is increased by 100%, making the tumor invisible, when the liver density is decreased by 40% for the original linear attenuation coefficient per pixel of liver, the value of the tumor density needed to make the tumor invisible was reduced to 10% increment for the liver activity.

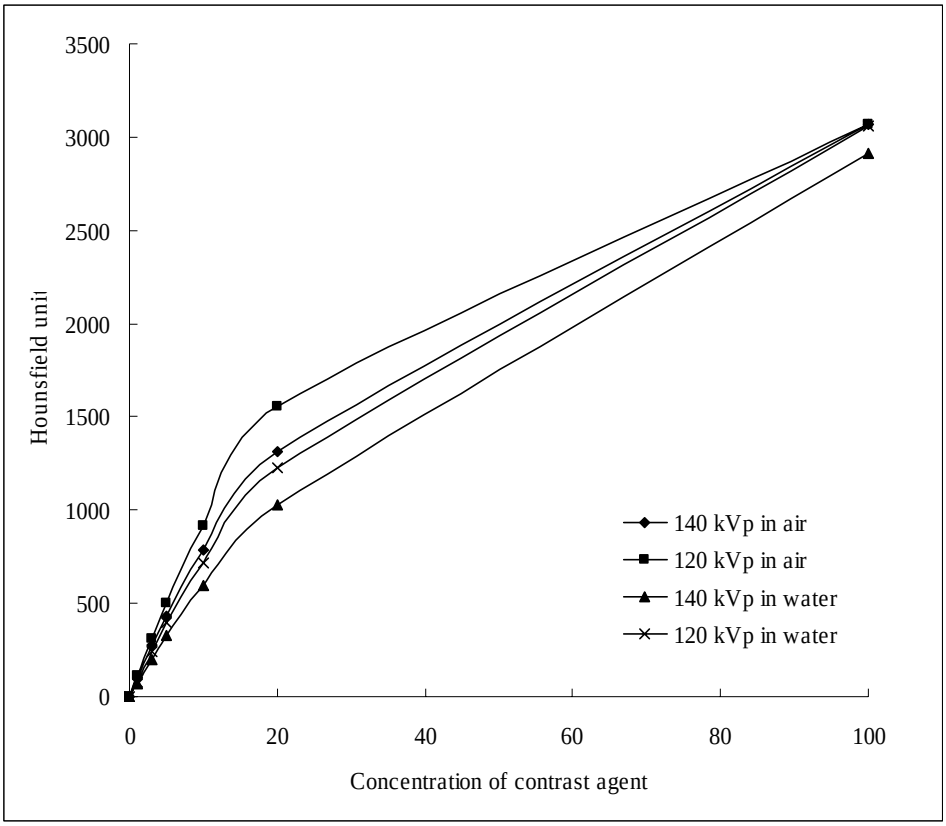

Figure 5.1. Concentration and tube voltage dependence of Hounsfield Unit for contrast agent.

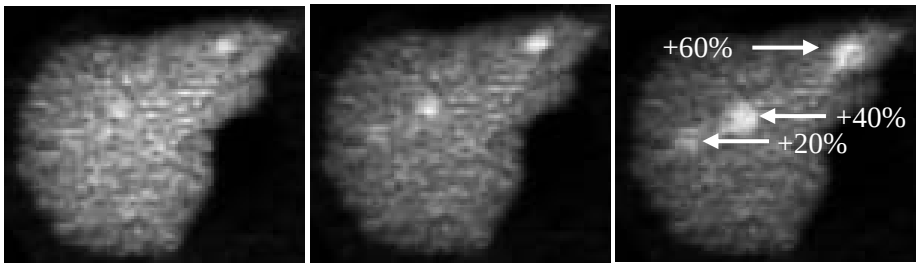

1.2 cm 1.6 cm 2.4 cm

Figure 5.2. Artifacts generated by the non-uniform enhancement of contrast agent on the transmission map. They depend on the concentration and size of non-uniformly distributed contrast agent.

Table 5.1. Signal to noise ratio between the artifacts introduced by the non-uniform enhancement of contrast agent and background area.

	SNR		
Concentration of non-uniform enhancement	Size of non-uniform enhancement		
	1.2 cm	1.6 cm	2.4 cm
+20 %	1.17	2.33	2.98
+40 %	2.74	5.72	6.01
+60 %	3.24	6.23	6.65

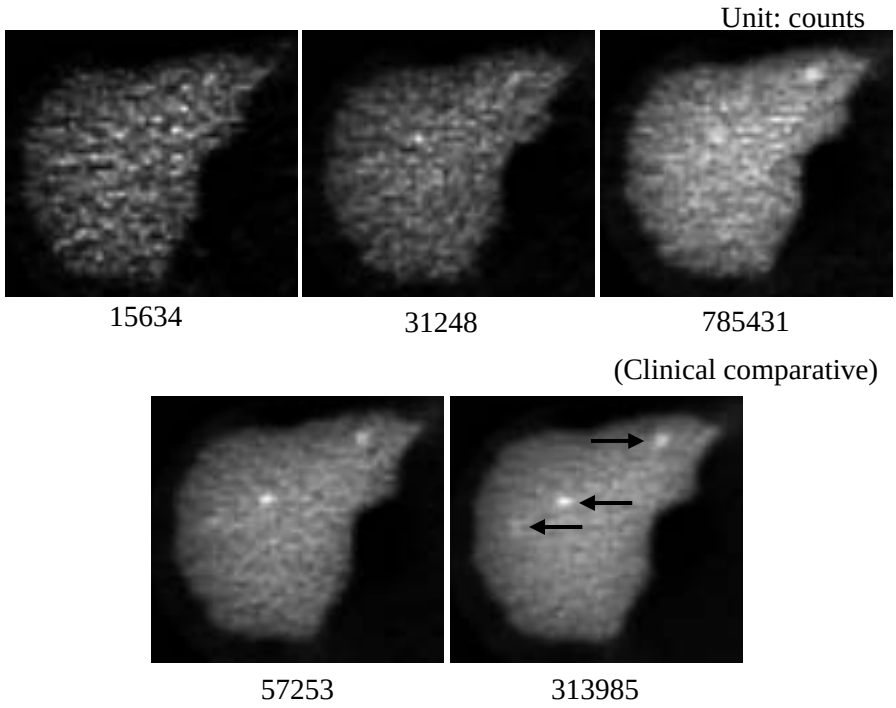

Figure 5.3. Emission images for a variety of noise values. Impact of the non-uniformly enhanced contrast agent is affected by the noise level, resulting in less evidence of the artifact as the count rate decreases.

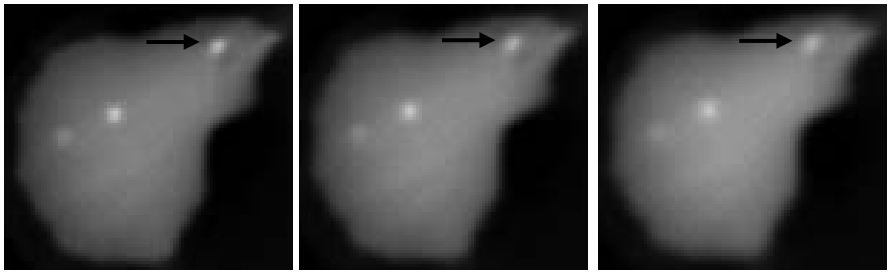

6 mm 8 mm 10 mm

Figure 5.4. Emission images with Gaussian smoothing of 6, 8, and 10 mm without noise component. Artifacts introduced by the non-uniform enhancement of contrast agent were less evident in the 10 mm than the 6 mm or 8 mm Gaussian smoothing.

Table 5.2. Maximum intensity values in the artifacts for each values of Gaussian smoothing. Artifact introduced by non-uniform enhancement increased by 40% for the liver density was used to measure the maximum intensity values. Poor resolution reduced the intensity of artifact.

Values of Gaussian smoothing	Maximum intensity values
6 mm	20.35
8 mm	18.59
10 mm	17.19

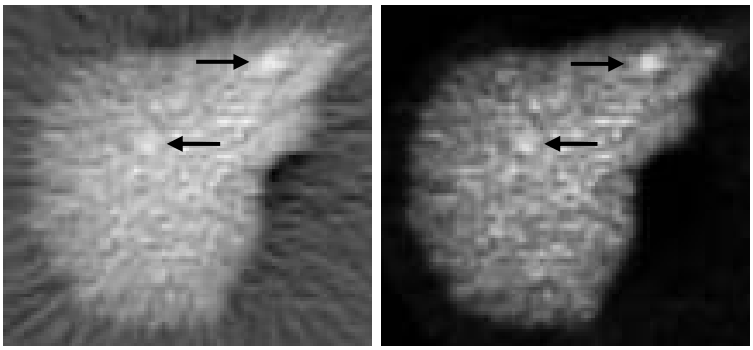

FBP OSEM

Figure 5.5. Emission images reconstructed by FBP and OSEM for the non-uniform enhancement of contrast agent. There was no visually discernable difference between both images in recognizing the artifact.

Table 5.3. Coefficient of variation for the images reconstructed by FBP and OSEM. The OSEM has a superior coefficient variation values than the FBP.

	CV (%)
FBP	15.11
OSEM	13.59

Table 5.4. Coefficient of variation and signal to noise ratio for tumors on the emission images corrected for attenuation with and without presence of contrast agent in the transmission map. The better coefficient of variation values and signal to noise ratio were acquired for the images corrected for attenuation with a uniform transmission map (without contrast agent).

	CV (%)	SNR
With contrast agent	10.74	7.56
Without contrast agent	9.34	8.48

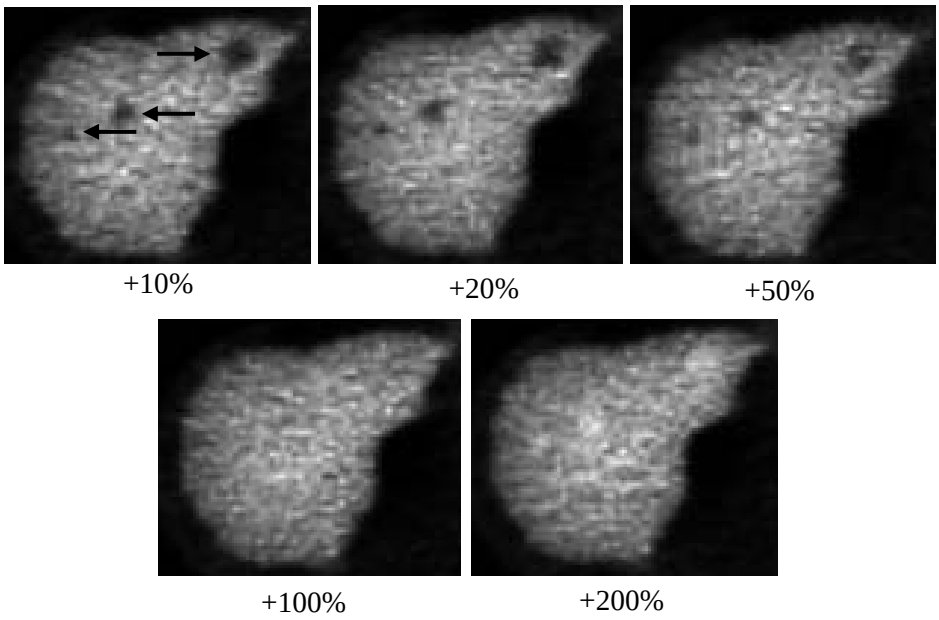

Figure 5.6. Emission images corrected for attenuation with the transmission map that is produced with hypo-attenuation of contrast agent. The tumor density on the emission map is changed by 10%, 20%, 50%, 100%, and 200% increments for the liver density. The intensity of tumors is affected by hypo-attenuation and also depends on the tumor density on the emission map. In this simulation, the tumors were not observable by hypo-attenuation at the tumor density increased by 100 % for the liver density.

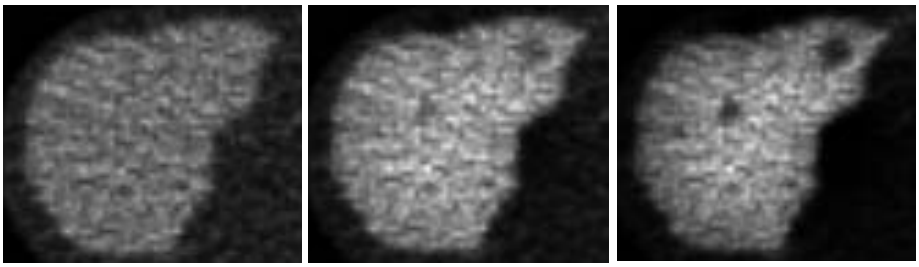

-40% (+10%) -20% (+20%) Original linear attenuation coefficient for the liver (+50%)

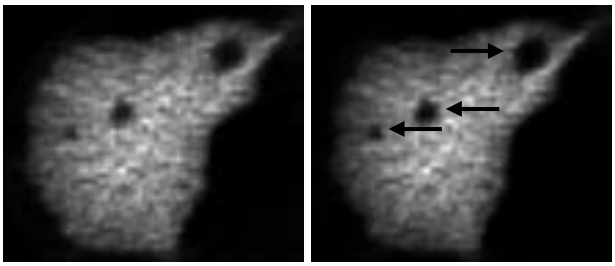

+20% (+100%) +40% (+200%)

Figure 5.7. Different time phases were simulated by changing the linear attenuation coefficient of liver to ± 20% and ± 40% for the original value on the transmission map. Compared to the situation where the value of the tumor density is increased by 100% for the liver activity in emission map, making the tumor invisible, when the linear attenuation coefficient of the liver is decreased by 40% of the original value, the value of the tumor density needed to make the tumor invisible was reduced to 10% increment for the liver activity in the emission map.

VI. DISCUSSION

Attenuation correction is the most important factor in both image quality and quantitative accuracy of PET and PET/CT scanning[1,2,7]. It is conventionally performed using a transmission scan acquired with a transmission source such as ^{68}Ge or ^{137}Cs. The CT transmission scan recently introduced for the attenuation correction can be used to derive information for the correction in the PET/CT system. This is advantageous because it has a short acquisition time and good noise characteristics[9,10].

Recently, artifacts caused by metallic materials and contrast agents have become an issue in the PET and PET/CT systems[12-29]. Metallic materials have been known to generate artifacts due to the high-density differences between them and their surrounding materials. This can result in inaccurate estimations of the attenuation coefficient[12-19]. Goerres[12,13] and Kamel[14] showed that dental metallic implants can cause artifacts on head and neck images with the PET and PET/CT scanning. In addition, metallic materials including hip prostheses, knee joint prostheses, and cardiac pacemakers can induce artifacts as well in attenuation-corrected PET images[15-19].

As the PET/CT system has been rapidly adopted in many institutions, contrast agents have been used for the CT scan. Previous researchers have shown that contrast agent can introduce artifacts by overestimation of 511 keV photon attenuation and overcorrection of images[20-26]. This is caused by currently available PET/CT systems that use a bilinear scaling method to convert different CT Hounsfield Unit into attenuation images at 511 keV without regard to the contrast agent that has a higher attenuation than soft tissue[9,20,24,27]. Correction method was proposed by Sadek et al for the contrast-induced artifacts using modified CT attenuation map[25]. However, the correction method for the contrast-induced artifacts has not been routinely established in clinical situation. Negative contrast agents[20,26] was also proposed to avoid artifacts induced by positive contrast agents. There have been conflicting reports on this subject. While some researcher reported that there was no significant effect caused by contrast agent[27-29], some others reported that artifacts were generated by contrast agent[20-26].

In agreement with previous studies[12-19], our simulation and experimental study demonstrated that aluminum and titanium structures can produce artifacts on the attenuation-corrected images. The results revealed that various

factors can affect the appearance of artificial increases, including the size and density of the metallic materials, the noise level, the image resolution, the amount of shift, and the transmission and emission processing.

The shape of the aluminum structure had no effect in the generation of artifacts, although further studies on a more variety of shapes need to be performed. Contrary to our results, Goerres et al.[15] demonstrated that the shape of the metallic hip prosthesis is important, since artifacts are only generated in the presence of a difference in shape between a high density metallic object and the surrounding tissues.

Artifacts are strongly influenced by the size of the metallic materials, because smaller objects were much more influenced by factors such as the noise component and image resolution. Larger objects were less influenced by these factors.

The more dense titanium produced stronger artifacts than the aluminum did. Poor resolution and a partial volume effect can cause the generation of artifacts through the inconsistency between high-density metallic materials and the surrounding tissues. This can result in the overcorrection of low-density areas[15]. Therefore, the more dense titanium can cause a bigger inconsistency with the

surrounding low-density materials, which can in turn result in the production of a stronger artifact compared to the artifacts produced by aluminum. Our results showed that titanium produced stronger artifacts than aluminum even for small sizes, shifts, and low count rates.

Artifacts generated by metallic materials were less evident at low count rates, while they were obvious at long acquisition durations. This indicates that high noise components can suppress the visibility of artifacts. Therefore, artifacts generated by metallic materials sometimes may not be found at short clinical acquisition durations, especially for the low density and the small size of metallic materials.

Our GE Advance PET and GE Discovery ST PET/CT systems have 6.2 mm and 4.8 mm of spatial resolution, respectively. Limited spatial resolution can affect the artifacts caused by metallic materials. Because of poor resolution, artifacts were less evident on the PET/CT images in our results, especially for the small size of metallic materials. However, there was no remarkable difference between the ^{68}Ge-based attenuation correction and the CT-based attenuation correction in introducing artifacts, although comparison is not direct between these totally different systems. Previous articles reported that

artifacts have different appearances between the ^{68}Ge-based attenuation correction images and the CT-based attenuation correction images in the GE Discovery LS PET/CT system[15]. The artifacts also showed a higher radioactivity concentration in the CT-based attenuation correction images than they did in the ^{68}Ge-based attenuation correction images[11, 12, 15, 17]. However, our results showed that the artifacts in the ^{68}Ge-based attenuation correction images have a visually higher intensity than in the CT-based attenuation correction images. This is caused by poor resolution of the PET/CT images, which results in a much more partial volume effect than images produced by PET.

Movement between the emission and transmission scans was a very important factor in introducing artifacts, since it led to a strong increase in artifact intensity. Low-density aluminum without movement did not produce artifacts even at a high-count rate, while movement between emission and transmission scans led to artifacts at a high-count rate. Artifacts were generated by titanium even at clinical acquisition duration without movement, because of high density of the titanium. The intensity of this artifact was strikingly increased by both movement and a high-count rate. Previous researchers found

similar results using metallic hip prosthetic materials[15].

Image quality can be influenced by reconstruction algorithms[6]. FBP provides rapid reconstruction time, but it may also generate streak artifacts and negative values. OSEM is one of the iterative reconstruction algorithms that provides improved spatial resolution and is free from streak artifacts. Our results illustrated that the images reconstructed by the OSEM produced relatively less noise, which resulted in better visibility than the images produced by FBP. However, there were no observable visual differences in the artifacts between the OSEM and FBP method.

Different attenuation correction methods of MAC and SAC based on ^{68}Ge transmission scans generated slightly different aspects in the artifacts. The images corrected using the SAC method degraded the intensity of artifacts compared to the images corrected by the MAC method. Kaneko et al.[34] reported similar results, that the use of the SAC method underestimates the attenuation correction coefficients and the ^{18}F activity concentration values when compared with the MAC method.

As mentioned previously, contrast agents which delineate anatomical structures in diagnostic CT scanning[26] may generate artifacts in the

attenuation-corrected PET images[20-26], since commercial PET/CT systems typically don't consider the contrast agent when they translate the x-ray energy to 511 keV γ-ray energy.

Our experimental results demonstrated that Hounsfield Unit depends on concentration of contrast agent and tube voltage. More attenuation is acquired in more dense concentrations. The Hounsfield Unit was higher at 120 kVp than 140 kVp for both air and water, when tube current is fixed. Therefore, it could be possible to expect that the more dense contrast agent at low tube voltages have higher probability in producing artifacts by more overcorrection than contrast agent with low density at higher tube voltage.

Non-uniform enhancement of contrast agent produced artifacts on the attenuation-corrected liver images. Our results demonstrate that inappropriate hyper-uptake could appear on the attenuation-corrected PET images, due to possible non-uniform enhancement of contrast agent, when the contrast agent is used for the CT scanning. Therefore, it is important to understand these possible artifacts to avoid false-positive detection. The impact of non-uniform enhancement of contrast agent is affected by various factors including the concentration and distribution size of contrast agent, the noise component, the

image resolution, and the reconstruction algorithm. These factors reduced the impact of contrast agent and thus may result in no considerable effect for some cases as shown in previous studies[27-29].

Hypo-attenuation of contrast agent in tumors resulted in degradation of tumor intensity on the attenuation-corrected PET images. While the tumors generally have high FDG uptake on PET images, contrast agent can be hypo-attenuated in the tumors. Thus, hypo-attenuated contrast agent can affect the intensity of the tumors on the CT-based attenuation-corrected PET images. Similar results caused by hypo-attenuation can possibly occur in the attenuation-corrected patient data, resulting in misreading. In addition, that degradation of the tumor intensity is influenced by different time phases, which emphasizes the importance of time point for CT acquisition.

Our simulation and experimental results for metallic materials and contrast agents suggested that it is quite important to understand the impact of metallic materials and contrast agents on attenuation-corrected PET and PET/CT images. Therefore, these effects need to be considered for qualitative and quantitative analysis for the attenuation-corrected images. Further study may be needed for clinical evaluation of the influence of metallic materials and

contrast agents in patient data.

VII. CONCLUSION

The combination of motion between transmission and emission scans and small dense structures can cause artifacts on attenuation-corrected PET and PET/CT images. The severity of these effects depends on a variety of factors, including the size and density of the metallic materials, the transmission and emission noise level, the image resolution, the amount of shift, and the transmission and emission processing. Contrast agents can cause artifacts and degrade image quality on attenuation-corrected PET/CT images. The severity of these effects depends on a variety of factors, including the concentration and distribution size of contrast agent, the noise levels, the image resolution, and the reconstruction algorithm. The non-uniform enhancement of contrast agent in transmission map produced inappropriate hyper-uptake on the attenuation-corrected emission images. Hypo-attenuation of contrast agent in tumors can degrade the tumor intensity on the attenuation-corrected emission images and degradation of the tumor intensity is influenced by different time phases.

Our simulation and experimental results indicated that the impact of metallic materials and contrast agents should be considered with a full understanding of

their potential problems in clinical PET and PET/CT images.

REFERENCES

1. Sandler MP, Coleman RE, Patton JA, Wackers FJT, Gottschalk A. Diagnostic nuclear medicine. 4th ed. Philadelphia (PA): Lippincott Williams & Wilkins; 2003.

2. Cherry SR, Sorenson JA, Phelps ME. Physics in Nuclear Medicine: 3rd ed. Philadelphia (PA): Saunders; 2003.

3. Phelps ME. PET: the merging of biology and imaging into molecular Imaging. J Nucl Med 2000;41(4):661-681.

4. Lundqvist H, Lubberink M, Tolmachev V. Positron emission tomography. Eur J Phys 1998;19:537-552.

5. Zanzonico P. Positron emission tomography: a review of basic principles, scanner design and performance, and current systems. Seminars in Nuclear Medicine 2004;XXXIV(2):87-111.

6. Son H-K, Yun M, Jeon TJ, Kim DO, Jung H-J, Lee J-D, et al. ROC Analysis of Ordered Subset Expectation Maximization and Filtered Back Projection Technique for FDG-PET in Lung Cancer. IEEE Trans Nucl Sci 2003;50(1):37-41.

7. Zaidi H, Hasegawa B. Determination of the attenuation map in emission tomography. J Nucl Med 2003;44:291-315.

8. Wahl RL. To AC or not to AC: that is the question. J Nucl Med 1999;40:2025-2028.

9. Kinahan PE, Townsend DW, Beyer T, Sashin D. Attenuation correction for a combined 3D PET/CT scanner. Med Phys 1998;25(10):2046-2053.

10. Burger C, Georres G, Schoenes S, Buck A, Lonn AHR, von Schulthess GK. PET attenuation coefficients from CT images: experimental evaluation of the transformation of CT into PET 511-keV attenuation coefficients. Eur J Nucl Med 2002;29:922-927.

11. Nakamoto Y, Osman M, Cohade C, Marshall LT, Links JM, Kohlmyer S, et al. PET/CT: comparison of quantitative tracer uptake between Germanium and CT transmission attenuation-corrected images. J Nucl Med 2002;43:1137-1143.

12. Goerres GW, Hany TF, Kamel E, von Schulthess GK, Buck A. Head and neck imaging with PET and PET/CT: artefacts from dental metallic implants. Eur J Nucl Med 2002;29(3):367-370.

13. Goerres GW, Schmid DT, Eyrich GK. Do hardware artifacts influence the performance of head and neck PET scans in patients with oral cavity squamous cell cancer?. Dentomaxillofacial Radiology 2003;32:365-371.

14. Kamel EM, Burger C, Buck A, von Schulthess GK, Goerres GW. Impact of metallic dental implants on CT-based attenuation correction in a combined PET/CT scanner. Eur Radiol 2003;13:724-728.

15. Goerres GW, Ziegler SI, Burger C, Berthold T, von Schulthess GK, Buck A. Artifacts at PET and PET/CT caused by metallic hip prosthetic material. Radiology 2003;226(2):577-584.

16. Heiba SI, Luo J-Q, Sadek S, Macalental E, Cacavio A, Rosen G, et al. Attenuation-correction induced artifacts in F-18 FDG PET imaging following total knee replacement. Clinical Positron Imaging 2000;3(6):237-239.

17. Visvikis D, Croasdale CI, Lonn AHR, Bomanji J, Gacinovic S, Ell PJ. CT-based attenuation correction in the calculation of semi-quantitative indices of [^{18}F]FDG uptake in PET. Eur J Nucl Med 2003;30:344-353.

18. Bujenovic S, Mannting F, Chakrabarti R, Ladnier D. Artifactual 2-deoxy-2-[18F]fluoro-D-glucose localization surrounding metallic objects in a PET/CT

scanner using CT-based attenuation correction. Molecular Imaging and Biology 2003;5(1):20-22.

19. Halpern BS, Dahlbom M, Waldherr C, Yap CS, Schiepers C, Silverman DH, et al. Cardiac pacemakers and central venous lines can induce focal artifacts on CT-corrected PET images. J Nucl Med 2004;45:290-293.

20. Antoch G, Freudenberg LS, Beyer T, Bockisch A, Debatin JF. To enhance or not to enhance? ^{18}F-FDG and CT contrast agents in dual-modality ^{18}F-FDG PET/CT. J Nucl Med 2004;45;56S-65S.

21. Nakamoto Y, Chin BB, Kraitchman DL, Lawler LP, Marshall LT, Wahl RL. Effects of nonionic intravenous contrast agents at PET/CT imaging: phantom and canine studies. Radiology 2003;227(3):817-824.

22. Cohade C, Osman M, Nakamoto Y, Marshall LT, Links JM, Fishman EK, et al. Initial experience with oral contrast in PET/CT: phantom and clinical studies. J Nucl Med 2003;44:412-416.

23. Antoch G, Freudenberg LS, Egelhof T, Stattaus J, Jentzen W, Debatin JF, et al. Focal tracer uptake: a potential artifact in contrast-enhanced dual-modality PET/CT scans. J Nucl Med 2002;43:1339-1342.

24. Antoch G, Jentzen W, Freudenberg LS, Stattaus J, Mueller SP, Debatin JF, et al. Effect of oral contrast agents on computed tomography-based positron emission tomography attenuation correction in dual-modality positron emission tomography/computed tomography imaging. Invest Radiol 2003;38:784-789.

25. Nehmeh SA, Erdi YE, Kalaigian H, Kolbert KS, Pan T, Yeung H, et al. Correction for oral contrast artifacts in CT attenuation-corrected PET images obtained by combined PET/CT. J Nucl Med 2003;44:1940-1944.

26. Antoch G, Kuehl H, Kanja J, Lauenstein TC, Schneemann H, Hauth E, et al. Dual-modality PET/CT scanning with negative oral contrast agent to avoid artifacts: introduction and evaluation. Radiology 2004;230:879-885.

27. Dizendorf E, Hany TF, Buck A, von Schulthess GK, Burger C. Cause and magnitude of the error induced by oral CT contrast agent in CT-based attenuation correction of PET emission studies. J Nucl Med 2003;44:732-738.

28. Dizendorf EV, Treyer V, von Schulthess GK, Hany TF. Application of oral contrast media in coregistered positron emission tomography-CT. AJR 2002;179:477-481.

29. Yau Y-Y, Chan W-S, Tam Y-M, Vernon P, Wong S, Coel M, et al. Application of intravenous contrast in PET/CT: does it really introduce significant attenuation correction error?. J Nucl Med 2005;46:283-291.

30. Beyer T, Antoch G, Blodgett T, Freudenberg LF, Akhurst T, Mueller S. Dual-modality PET/CT imaging: the effect of respiratory motion on combined image quality in clinical oncology. Eur J Nucl Med Mol Imaging 2003;30:588-596.

31. Goerres GW, Burger C, Schwitter MR, Heidelberg TH, Seifert B, von Schulthess GK. PET/CT of the abdomen: optimizing the patient breathing pattern. Eur Radiol 2003;13:734-739.

32. Berger MJ, Hubbell JH, Seltzer SM, Coursey JS, Zucker DS. *XCOM: Photon Cross Section Database* (version 1.2). [Online] Available: http://physics.nist.gov/xcom. National Institute of Standards and Technology, Gaithersburg, MD. 1999.

33. Brancatelli G, Baron RL, Peterson MS, Marsh W. Helical CT screening for hepatocellular carcinoma in patients with cirrhosis: frequency and causes of false-positive interpretation. AJR 2003;180:1007-1014.

34. Kaneko K, Kuwabara Y, Sasaki M, Koga H, Abe K, Baba S, et al.

Validation of quantitative accuracy of the post-injection transmission-based and transmissionless attenuation correction techniques in neurological FDG-PET. Nucl Med Comm 2004;25:1095-1102.

ABSTRACT (IN KOREAN)

정량적 양전자방출단층촬영 영상에서 물리적 인자가 감쇠 보정에 미치는 영향

<지도교수 김희중>

연세대학교 대학원 의과학과

손혜경

양전자방출단층촬영 (PET)은 인체 내에서의 생물학적 과정을 양전자를 방출하는 방사성의약품을 이용하여 가시화하고 정량화할 수 있는 독특한 핵의학 영상 기법이다. PET은 비침습적으로 질병의 진단, 예후판정, 병변의 시기결정, 치료효과의 모니터링 등을 가능하게 하는 장점을 가지고 있다. 이러한 PET 영상의 정확도를 개선하기 위해서는 감쇠보정이 반드시 이루어져야 하며, 이는 ^{68}Ge 또는 ^{137}Cs 등을 이용한 투과 스캔을 통해 수행할 수 있다. 양전자방출단층촬영/전산화단층촬영 (PET/CT)은 근래에 들어 급속도로 보급되고 있는 최첨단 핵의학 영상 기기로서, 하드웨어적으로 기능적 영상과 해부학적 영상의 융합을 가능하게 한다. PET/CT 시스템의 CT 투과 영상 또한 감쇠 보정을 위해 사용할 수 있다. 그러나 최근 들어 금속성 물질 또는 조영제와 같은 물리적 인자가 감쇠 보정한 PET 또는 PET/CT 영상에서 인공산물을 발생시킬 수 있다는 연구 결과들이 보고 되고 있다. 본 연구의 목적은 감쇠 보정한 PET 영상에서 금속성 물질과 조영제가

영상에 미치는 영향을 연구하고자 하는 것이었다. 방출 스캔과 투과 스캔 간에 움직임이 있을 경우 알루미늄과 티타늄으로 인해 발생하는 인공산물의 영향을 평가하기 위해 모의 실험과 팬텀 실험을 수행하였다. 이 때 금속성 물질의 크기와 밀도, 투과 스캔과 방출 스캔의 잡음 정도, 해상도, 움직임 정도, 투과 영상과 방출 영상의 처리 등의 다양한 인자들에 대하여 평가하였다. 조영제에 의한 영향을 평가하기 위해 모의 실험과 팬텀 실험을 수행하였다. 이 때 조영제의 비 균일 분포, 잡음 정도, 해상도, 투과 영상과 방출 영상의 처리, 조영제의 저 감쇠, 시간 별 조영제의 분포 차이 등의 다양한 인자들에 대하여 평가하였다. 투과 스캔과 방출 스캔 간의 움직임과 밀도가 높은 금속성 물질과의 조합은 감쇠 보정된 PET 영상에서 인공 산물을 발생시킴을 확인할 수 있었다. 금속성 물질에 의한 인공산물의 발생은 방출 스캔과 투과 스캔 간의 움직임 정도, 금속성 물질의 크기 및 밀도, 방출 영상과 투과 영상의 잡음 정도, 그리고 방출 영상과 투과 영상의 처리 방법 등 다양한 인자들에 의존함을 알 수 있었다. 조영제의 분포가 CT 영상에 잔존할 경우 이를 이용한 PET 영상의 감쇠 보정이 인공산물을 생성할 수 있고, 방출 영상의 질에 영향을 미침을 알 수 있었다. 이러한 조영제의 영향은 조영제의 밀도와 분포된 크기, 영상의 잡음 정도, 영상의 해상도, 그리고 재구성 알고리듬 등 다양한 인자들에 의존하는 것으로 나타났다. 투과 영상에서의 조영제의 비 균일 분포가 감쇠 보정한 방출 영상에서 인공 산물을 생성함을 확인할 수 있었다. 종양에서의 조영제의 저 감쇠가 감쇠 보정한 방출 영상에서 종양의

세기를 감소 시키는 것으로 나타났고, 이것은 시간 차에 따른 조영제의 분포 정도에 영향을 받는 것을 알 수 있었다. 금속성 물질과 조영제에 관한 본 연구의 결과로부터 이러한 물리적 인자들로 인해 발생할 수 있는 PET 또는 PET/CT 영상에서의 잠재적 문제에 대한 충분한 이해와 이에 대한 고려가 반드시 있어야 할 것으로 사료된다.

핵심되는 말: PET, PET/CT, 감쇠보정, 인공산물, 금속성 물질, 조영제